Rev. Adv. Mater. Sci. 44 (2016) 238-256

REVIEW ON IMPROVEMENTS IN SURFACE PERFORMANCE OF TiAl-BASED ALLOYS BY DOUBLE GLOW PLASMA SURFACE ALLOYING TECHNOLOGY

Naiming Lin[1,2], Jiaojuan Zou[1], Maolin Li[3], Junwen Guo[1], Yong Ma[1], Zhenxia Wang[1], Zhihua Wang[2], Xiaoping Liu[1] and Bin Tang[1]

[1]Research Institute of Surface Engineering, Taiyuan University of Technology, Taiyuan, 030024, P. R. China
[2]Shanxi Key Laboratory of Material Strength and Structure Impact, Taiyuan University of Technology, Taiyuan, 030024, P R China
[3]Nuclear and Radiation Safety Center, Ministry of Environmental Protection, Beijing 10082, P R China

Received: September 21, 2015

Abstract. TiAl-based alloys are one kind of innovative high temperature materials which have been extensively applied in aviation, space flight, military industry and other industrial sectors due to their high strength to weight ratio and other positive merits. However, insufficient wear resistance and poor oxidation resistance have restricted their much wider applications. Double glow plasma surface alloying (DGPSA) process has been confirmed as an effective surface modification technology to improve the surface performance of TiAl-based alloys. In this paper, the studies and applications of DGPSA process in improving the surface performance of TiAl-based alloys were reviewed and summarized.

1. INTRODUCTION

TiAl-based alloys (referred to TiAl alloys hereafter) are one kind of promising high temperature structural materials for aerospace and automobile industries due to their advantages, such as low density, high strength at elevated temperatures, excellent corrosion resistance, promising creep resistance and good mechanical properties [1-8]. TiAl alloys offer the opportunity for substantial weight savings when they were compared with Ni-based super-alloys assigned for similar structural applications [4]. However, their insufficient wear resistance and poor oxidation resistance become the major obstacles for their wider applications [9]. Accordingly, improving the wear resistance and high temperature oxidation resistance of TiAl alloys has received extensive attentions [10]. It has been well accepted that failure/degradation of material in engineering, e.g. wear or corrosion is mainly lies in the surface properties of the material rather than by bulk capabilities. Meanwhile the surface treatment can provide a promising compromise between the cost and the performance of engineering units [11]. For that surface treatment has been considered as an effective and suitable method to overcome the aforementioned problems for metallic materials [12]. A variety of surface techniques, such as surface hardening (shot/laser peening, surface nanocrystallization) [13-16], surface alloying (with non-metallic elements (NME) or metallic elements (ME)) [17-25], plasma electrolytic modification [26-30], physical vapor deposition (PVD) [31-35], electrodeposition [36-39], spraying [40-42], sol-gel method [43-45], electro spark deposition (ESD) [46,47], laser surface treatment [48-50], ion implantation [51-53], thermal oxidation [54], current heating [55, 56], electron beam irradiation [57,58], glass protection [59], also sev-

Corresponding author: Naiming Lin, e-mail: lnmlz33@126.com

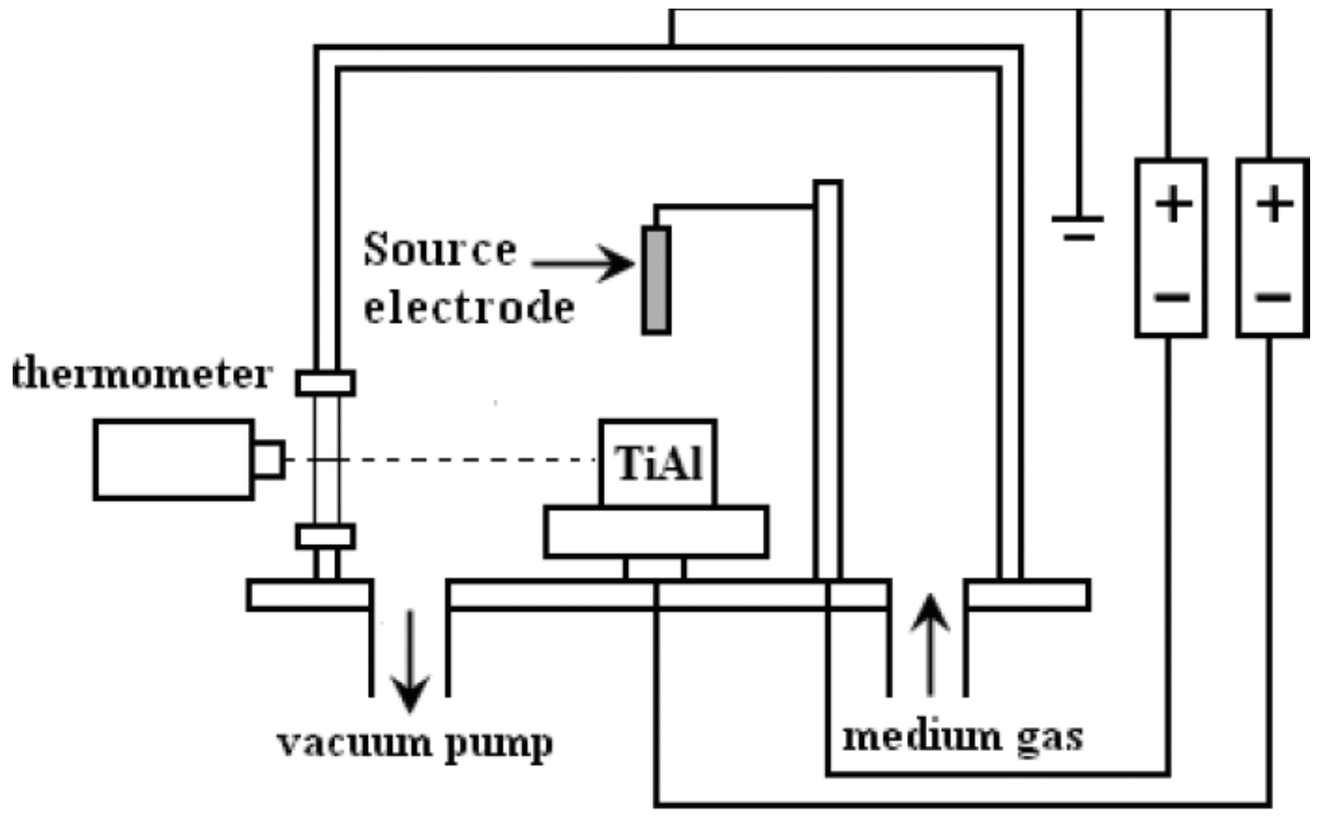

Fig. 1. Schematic diagram of DGPSA apparatus.

eral duplex treatments have been conducted to enhance the wear and oxidation resistance of TiAl alloys [60-64]. Most of the applied surface treatment techniques with various technological principles have been succeeded in improving the surface performance of TiAl alloys under different service conditions; actually the techniques also have their own benefits and shortcomings.

Surface alloying which is realized by solid phase/liquid phase/vapor phase processes can enhance the surface hardness, improve the surface performance against wear and corrosion of the substrate with less alloying elements than bulk alloying, as well as obtain a strong metallurgical bond between the alloying layer and the substrate. Double glow plasma surface alloying (referred to as DGPSA in the following) which is also called as Xu-Tec/Xu-Loy process had been covered by US and other international patents more than 30 years ago [65]. In fact the DGPSA was evolved on the basis of plasma nitriding and sputtering effect during the studies on ion nitriding of Ti6Al4V titanium alloy [66,67]. The DGPSA is able to realize surface alloying via both NME and ME as alloying elements. The DGPSA processes contain single element alloying, alloying with single NME or ME; binary element alloying, existing NME + NME, NME + ME and ME + ME; also minor research of ternary alloying has been carried out.

In this review, the technological principle of DGPSA was firstly introduced in brief, and the application status of DGPSA process for improving the surface performance of TiAl alloys was reviewed and summarized. This work is expected to create database and provide reference information, thereby broadening practical applications of DGPSA on TiAl alloys or Ti-based metallic materials.

2. TECHNOLOGY RESEARCH STATUS

2.1. The principle of the DGPSA process

The DGPSA was originally developed based on the plasma nitriding and sputtering technique. A bell chamber equipped with a complete vacuum system is necessary. Fig. 1 presents the schematic diagram of DGPSA apparatus. In the vacuum chamber, the object (work piece) and the so called source electrode (made up of one or more desired alloying elements) are two negatively charged members and the anode is the earthed vacuum bell jar. As suggested in Fig. 1, when the two power supplies were turned on and reached certain voltage values, both cathode and source electrode would envelop with glow discharge under the argon plasma atmosphere. One glow discharge heats the object to be alloyed. While the second glow discharge bombards the source electrode to sputtering out the desired alloying elements.

This phenomenon was named as the “double glow discharge”. The charged ions or particles which are bombarded from the source electrode migrate to and firstly diffuse into then deposit onto the surface of the object under the influence of an electric field, and then obtaining an alloyed surface. The thickness values of the surface alloying layers vary from several micrometers to 500 μm, with alloying elements in a concentration of a few percent to 90% or even more. Prof. Zhong Xu and his group in Taiyuan University of Technology (TYUT, Taiyuan, P. R. China) accidentally discovered this phenomenon during the plasma nitriding trials of Ti6Al4V titanium alloy in early-1980s, and then developed

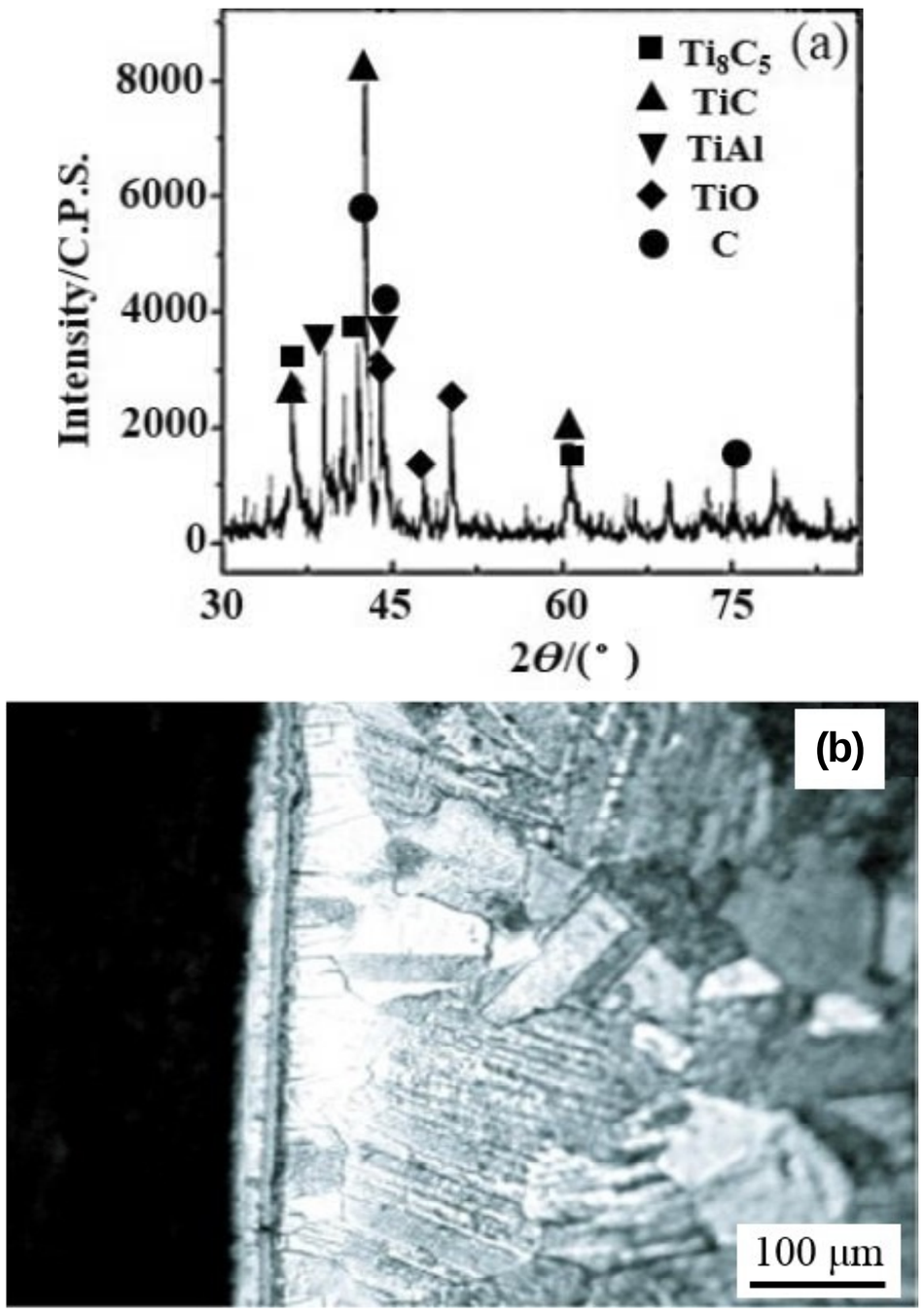

Fig. 2. XRD pattern (a) and metallograph (b) of carburized layer on γ-TiAl.

and named the so called “DGPSA” process [66,67]. Nearly three decades past several most important features of DGPSA have been summarized as follows: (1) resource and precious metal element conservation, (2) free of pollution, (3) controlled alloy composition on the surface, (4) wide range selection of alloying elements, (5) gradient distributions of the composition and property, (6) holding a metallurgical bond between alloying layer and substrate. Since the double glow discharge phenomenon was discovered, great deals of studies on DGPSA processing were conducted to refine the composition or microstructure in the near surface and enhance the surface properties, such as corrosion resistance, wear resistance and resistance to high temperature oxidation of Fe-based and Ti-based materials under different conditions in the past three decades [66,67].

3. STUDIES AND APPLICATIONS OF DGPSA ON TiAl ALLOYS

3.1. DGPSA with single element

In this section, DGPSA on TiAl alloys using carbon (C), chromium (Cr), molybdenum (Mo), niobium (Nb) and tungsten (W) were introduced.

The formation of hard carbides in carburized layer obtained by DGPSA was helpful to improve the tribological performance of TiAl alloys. Ma et al. [68] applied DGPSA to realize hydrogen-free carburizing of g-TiAl and had significantly improved the tribological properties of ã-TiAl. The continuous and compact carburized layer was composed of Ti_8C_5, TiC, TiAl and C; it had reached an effective thickness of about 15 mm (see Fig. 2).

Yuan et al. [69] modified Ti_2AlNb alloy via DGPSA carburizing (at 950 °C for 3 h) to improve its wear resistance. It was found that about 11 μm carburized layer was obtained on the Ti_2AlNb alloy surface (Fig. 3a), and the content of carbon gradually decreased from the surface to the matrix (Fig. 3b). The main phases of the carburized layer were C, TiC, and Ti_2AlC (Fig. 4). The surface dynamic microhardness of the carburized layer is 9.61 GPa. The specific wear rate of the carburized sample is only 1.82 % of the matrix alloy. The wear trace of the carburized layer was narrower and shallower than that of Ti_2AlNb alloy (Figs. 5 and 6), which meant the wear resistance of Ti_2AlNb alloy was greatly increased after DGPSA carburization treatment.

Yang et al. [70] conducted DGPSA carburizing (at 1100 °C for 3 h) on Ti_2AlNb base O phase alloy

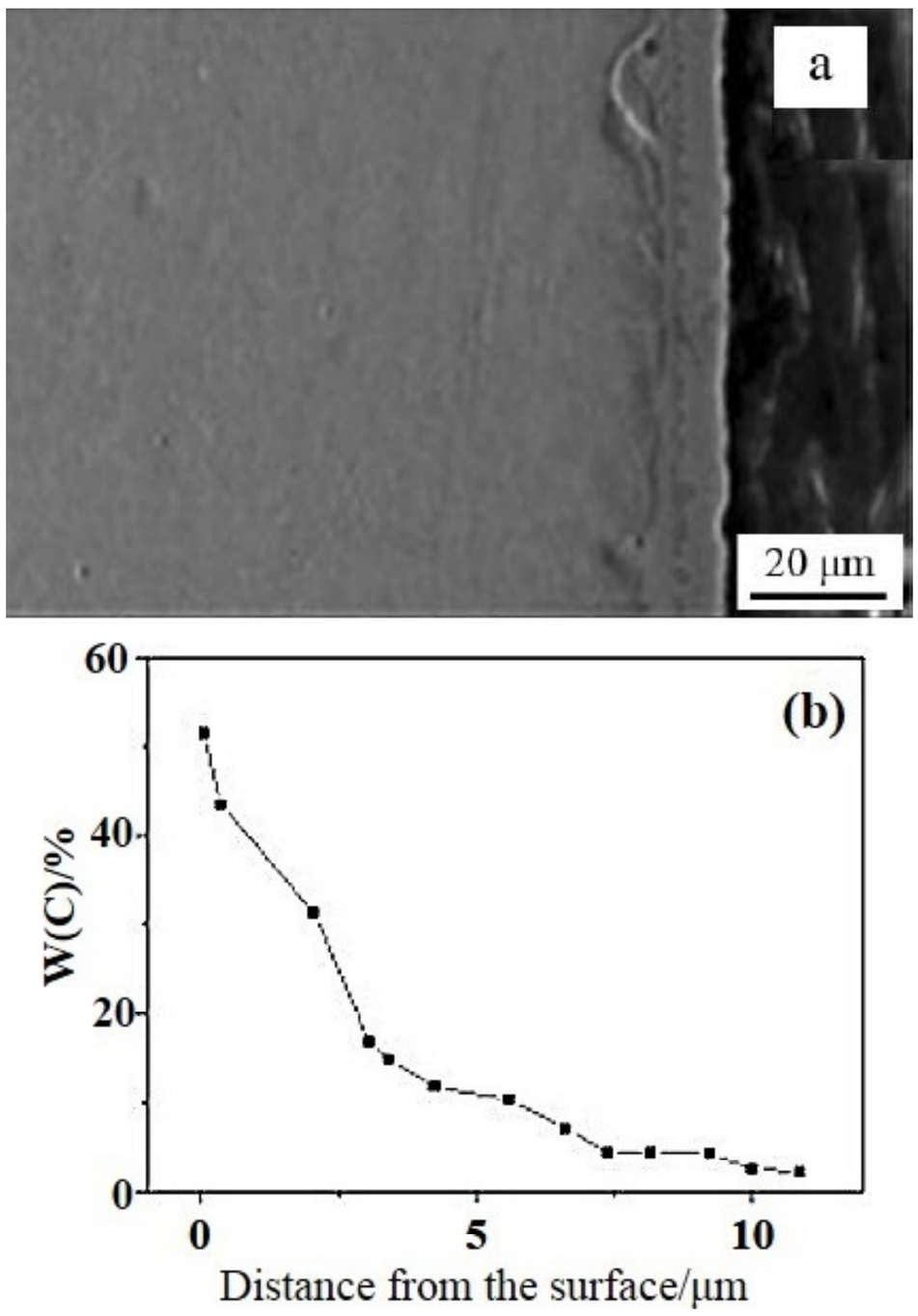

Fig. 3. Cross-sectional microstructure (a) and composition profile of carburized layer (b) on Ti_2AlNb.

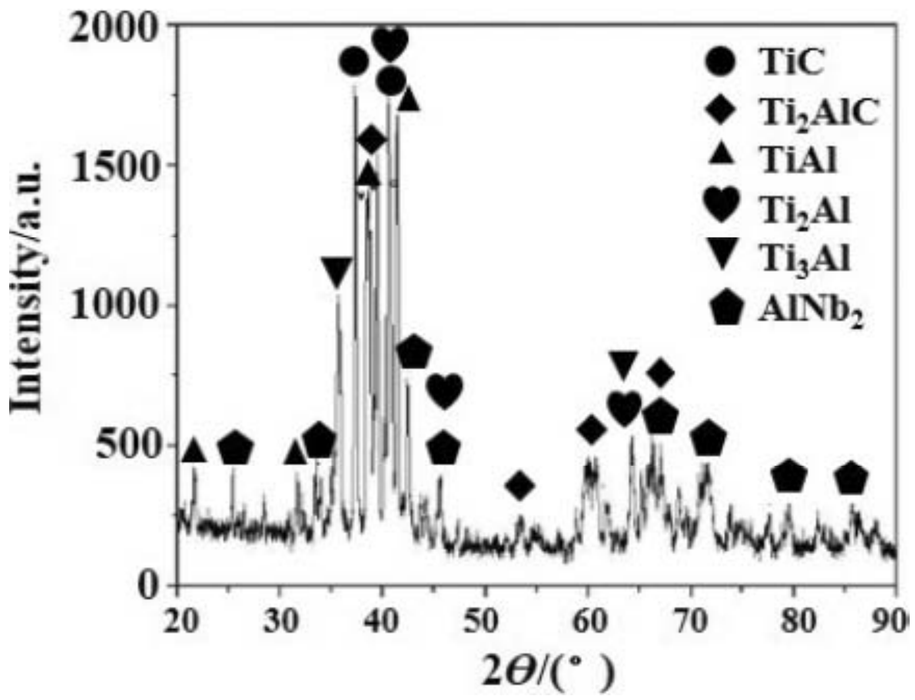

Fig. 4. XRD pattern of carburized layer on Ti_2AlNb.

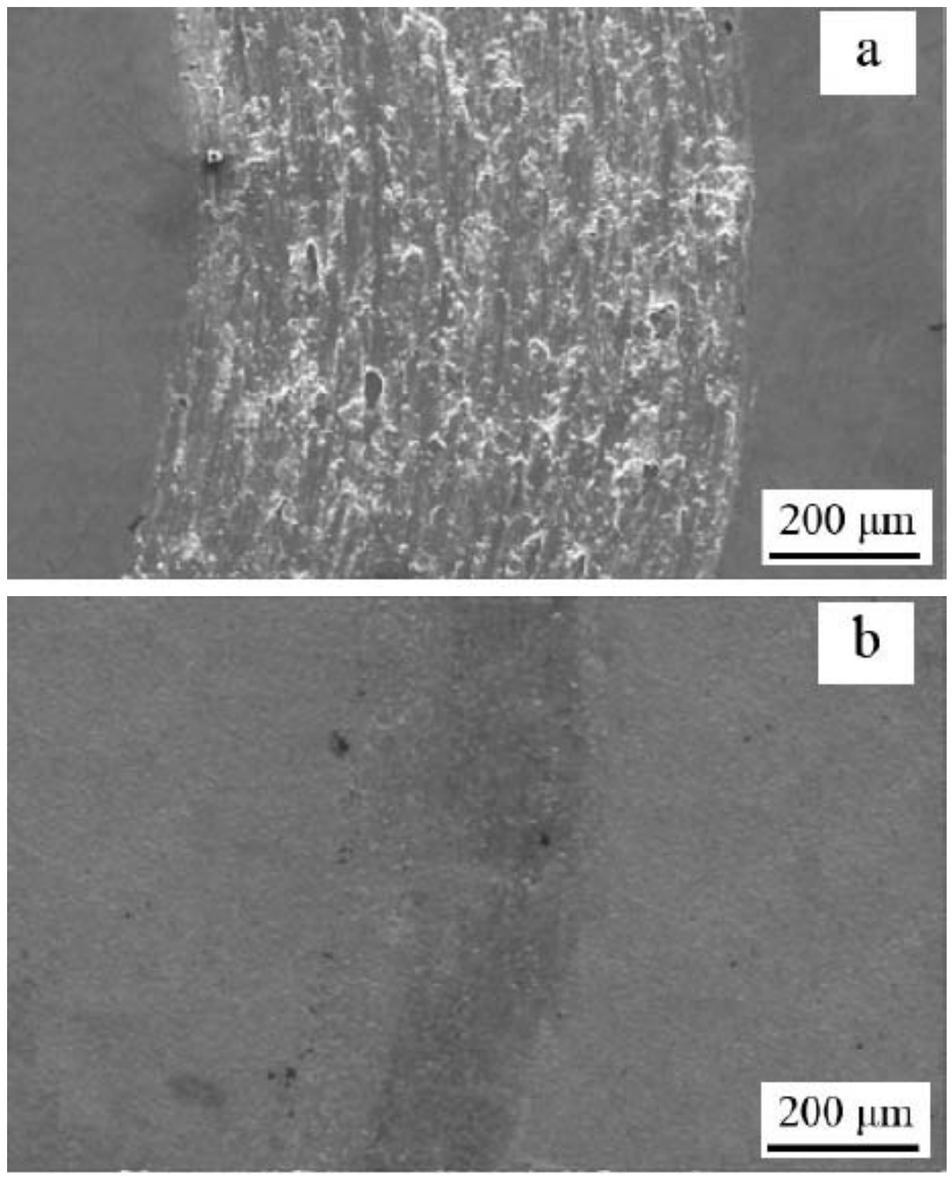

Fig. 5. Wear scars of Ti_2AlNb (a) and carburized layer (b).

to improve its wear resistance. The results showed that a 30 μm thick carburized layer was formed, and surface hardness of the carburized layer was 1053 $HV_{0.1}$ and the hardness values gradually decreased along the depth below the surface. The general friction coefficients of the carburized layer and matrix were 0.4 and 0.75, respectively. The specific wear rate of carburized layer is 1/17 of the matrix. The wear resistance of Ti_2AlNb alloy was significantly improved by DGPSA carburizing.

Zheng et al. [71] employed DGPSA to carry out chromizing of TiAl intermetallic aimed to get the key process parameters which were beneficial to against oxidation at high temperature. Experimental results indicated that the optimal values of key process parameters are as follows: the source electrode

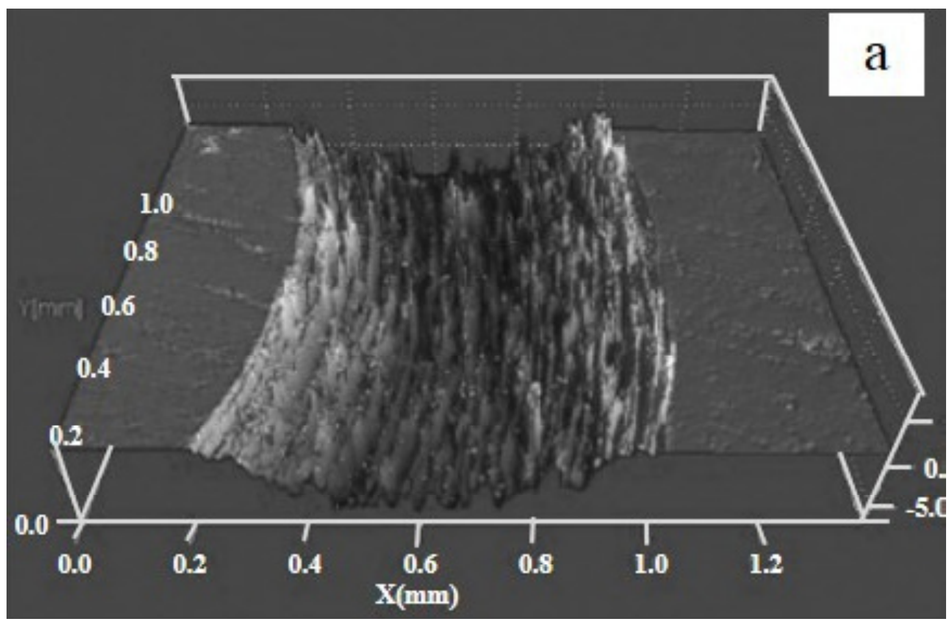

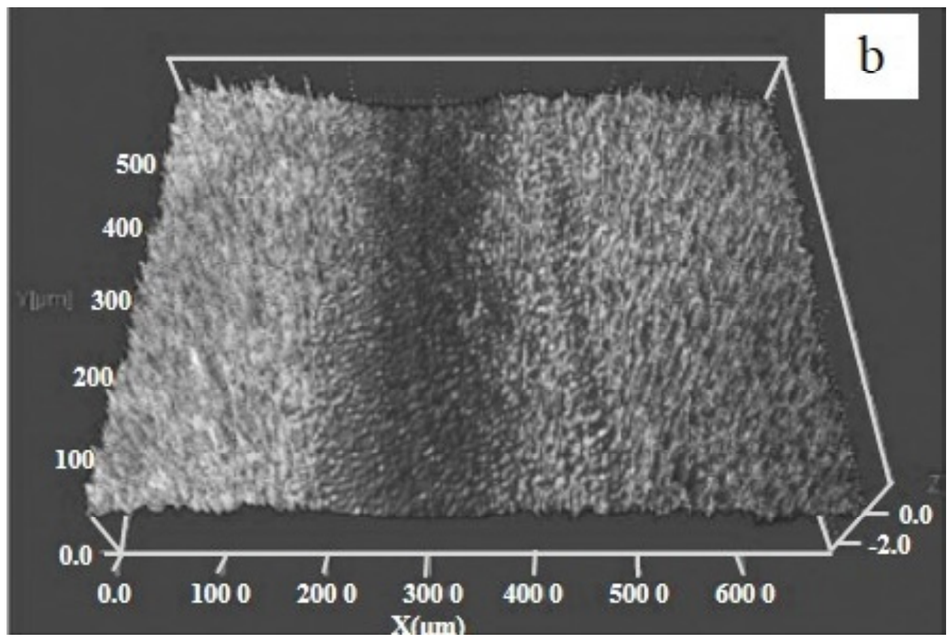

Fig. 6. 3D surface profilometry of the wear traces: Ti_2AlNb (a) and carburized layer (b).

voltage was -1300~-1200 V, the work piece voltage was -300~-200 V, the valid power density ratio is 4~5 and the gas pressure is 25~30 Pa. Wang et al. [72] obtained a harder chromizing coating via DGPSA under the following conditions: the source electrode voltage 700 V, the work piece voltage -450~-280 V, the distance between the source electrode and the work piece 18 mm and the gas pressure 25 Pa at 1050 °C for 4 h.

Ma et al. [73] performed chromizing on the surface of γ-TiAl alloy using DGPSA. The results showed that the chromized layer with an effective thickness of about 35 mm had firmly bonded to the substrate. The composition and micro-hardness degree of the chromized layer displayed gradient distribution from the surface to the substrate. Meanwhile the friction and wear resistance of γ-TiAl alloy were greatly enhanced.

He et al. [74] conducted DGPSA to form a layer of TiAl-Cr alloy on the surface of a TiAl-based alloy. The feasibility of the alloying process was evaluated by a first principle calculation method (see Fig. 7). The preparation process was optimized by investigating the effects of processing temperature and discharge pressure on the formation of surface alloy. The calculation using the first-principle method showed that the addition of Cr into the TiAl lattice would increase the stability of the system, and im-

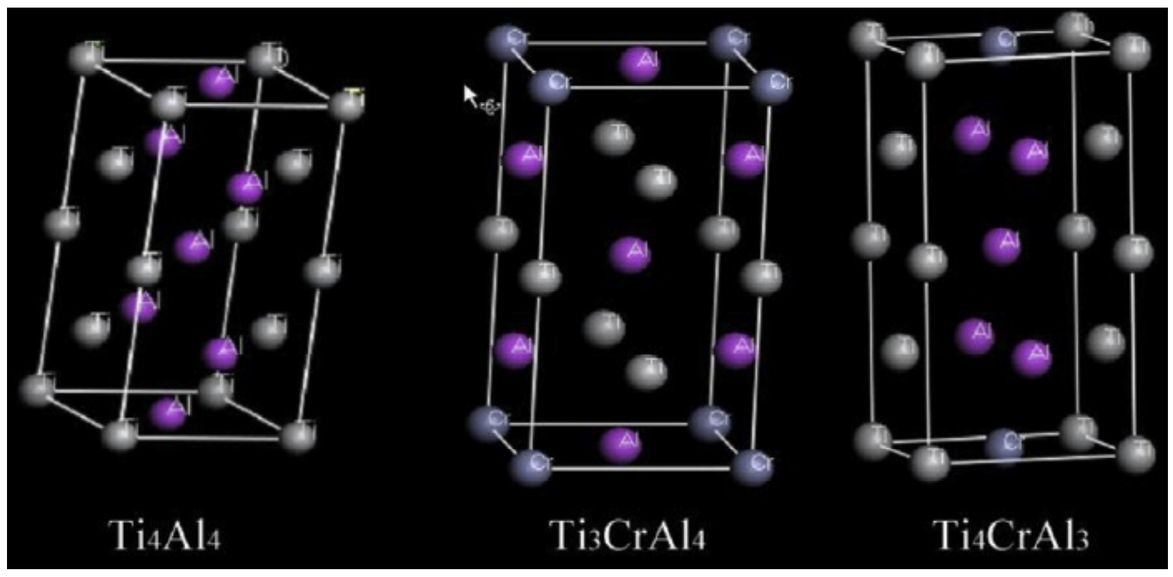

Fig. 7. The supercell models of TiAl with Cr addition.

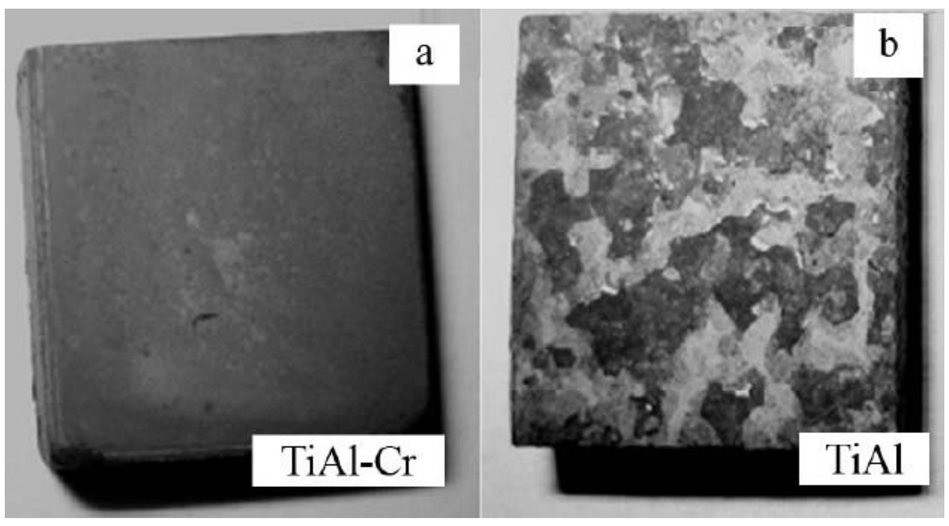

Fig. 8. Surface appearance of TiAl-Cr (a) and TiAl (b) after oxidized at 900 °C for 100 h.

prove mechanical properties of the alloy. The processing temperature was selected at 1100 !, slightly below the eutectic temperature of the Ti-Al system, which could ensure diffusion efficiency and also avoid the degradation of substrate microstructure. The optimum discharge pressure was 25 Pa within the range of 12~55 Pa. Sputtering and diffusion were well coordinated at this pressure and the obtained alloyed layer had the largest thickness.

He et al. [75] prepared TiAl-Cr alloy by DGPSA process to improve oxidation resistance of γ-TiAl alloy (Fig. 8). The oxidation kinetics of the TiAl-Cr surface alloy and the bulk γ-TiAl were examined. The scale of TiAl-Cr surface alloy initially was mainly consisted of Cr_2O_3, then composed of Cr_2O_3, Al_2O_3, and TiO_2, and eventually was the mixture of Al_2O_3 and TiO_2. The oxide scale was dense and integrated throughout the oxidation process. The realized improvement was owing to the enhancing of scale adhesion and the preferential oxidation of aluminum brought by the alloying effects of chromium.

Liang et al. [76] employed DGPSA process to realize chromizing of Ti_2AlNb, as well as improve its wear resistance. The process was conducted according to the following parameters: the working pressure 40~50 Pa, the source electrode voltage -1100~-800 V, the work piece voltage -600~-300 V, the distance between the source electrode and the work piece 18 mm, under 1000 °C for 4 h. The results indicated that the thickness of the chromized layer reached 30 μm. The surface content of Cr was about 38 wt.% and decreased in gradient along the distance from the surface to internal of substrate. The Cr was existed in the form of Al_5Cr_8, Cr_2Nb, and Cr_2Ti in the chromized layer. The chromized layer showed a higher surface hardness of above 950 HV than that of Ti_2AlNb matrix. The average friction of chromized layer was about 0.10, much lower than that of Ti_2AlNb matrix. The mass loss in wearing of chromized layer was just one twentieth of Ti_2AlNb matrix.

Wu et al. [77-81] enhanced the wear resistance of Ti_2AlNb by DGPSA chromizing process. The optimum process parameters: 970 °C for temperature, 4 h for chromizing time, and 30 Pa for gas pressure were favorable to obtain the required 100 μm thick chromized layer with the fine and uniform microstructure, high surface hardness and excellent wear resistance (Figs. 9-11). The chromized layer consisted of Cr-rich phases (Al_8Cr_5 and Cr_2Nb), and the content of chromium decreased gradually as the distance increased from the surface to the substrate. The wear rate of the chromized layer was approximately 2.4-fold and 1.2-fold lower than that of the substrate at either room temperature and 500 °C. The friction coefficient of the chromized layer at high temperature was the lowest, which was about 3-fold lower than that of the substrate. This may be attributed to the high micro-hardness and excellent bending strength between the chromized layer and the substrate, as well as the influence of slight oxidation. Better wear resistance and lower friction coefficient were contributed from the formation of Al_8Cr_5 and Cr_2Nb with high hardness and the hexagonal structure.

Liang et al. [82,83] conducted DGPSA molybdenizing on Ti_2AlNb alloy improve the wear resistance of the Ti_2AlNb orthorhombic alloy. It was found that both the processing temperature and the holding time had significant effects on the DGPSA

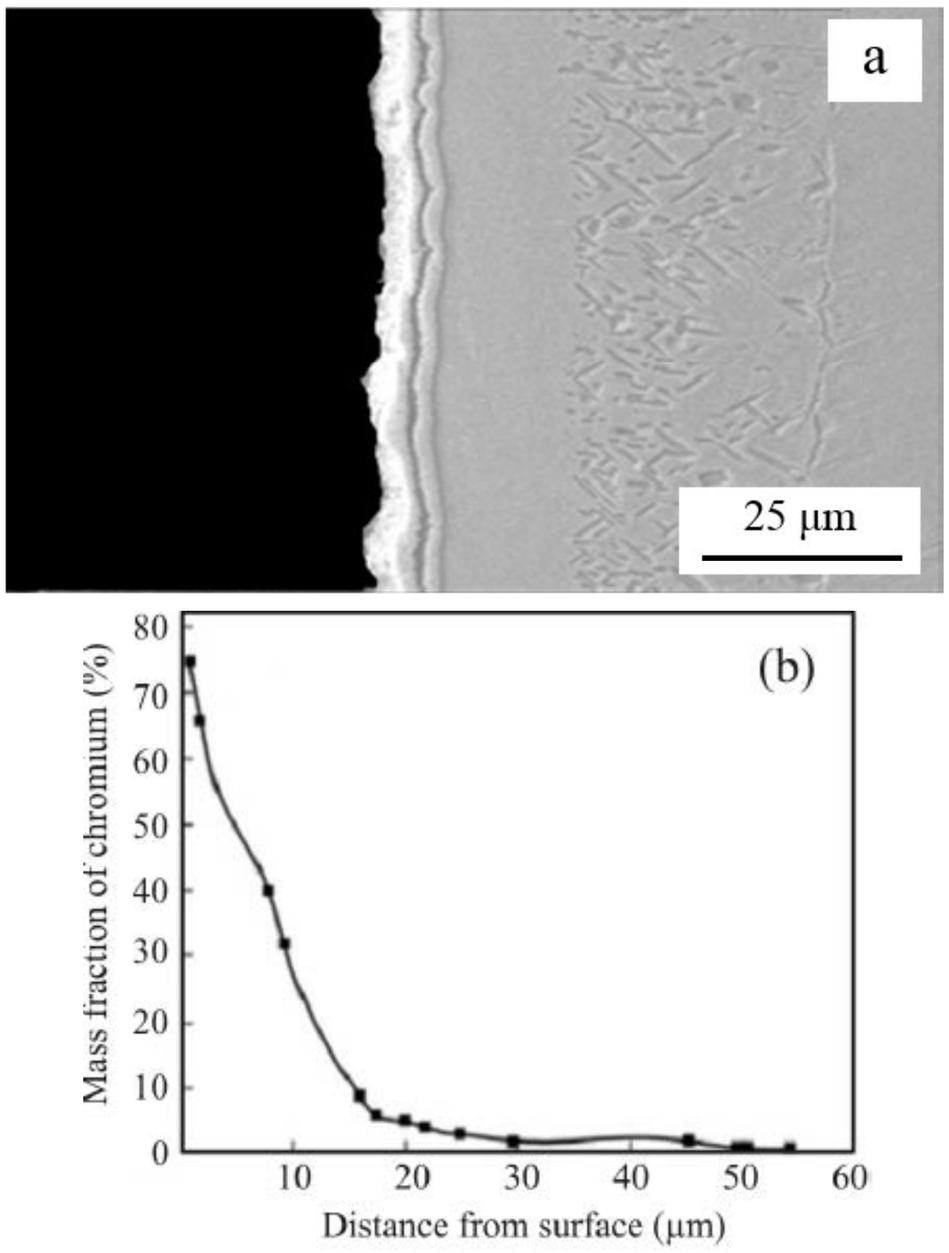

Fig. 9. Cross-sectional microstructure (a) and composition distribution (b) of chromized layer on Ti_2AlNb.

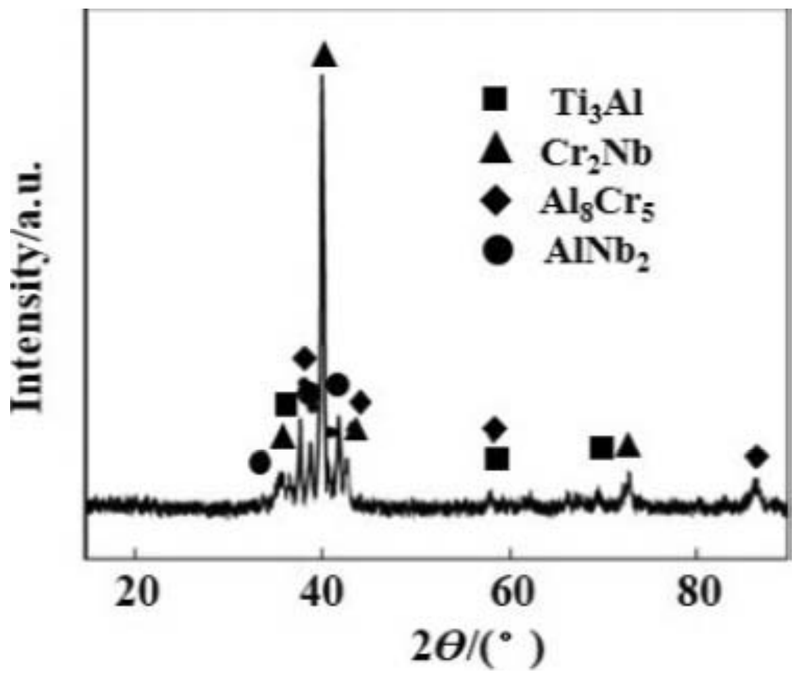

Fig. 10. XRD pattern of chromized layer on Ti_2AlNb.

process. The results indicated that elevating temperature accelerated the Mo diffusion in DGPSA molybdenizing. While a temperature above 1000 °C was unbeneficial to diffusion due to a phase transition. Prolonging of processing time could increase the thickness of molybdenized layer. When DGPSA molybdenizing at 980 °C, the diffusion coefficient of Mo in Ti_2AlNb was about 5.4×10^{-17} m^2/s. A molybdenizing layer was formed under the following processing parameters: the gas pressure 40~50 Pa, the source electrode voltage -1100~-800 V, the work piece voltage -600~-300 V, the distance between the source electrode and the work piece 15 mm, molybdenizing temperature 980 °C for 3 h time. The uniform and compact layer composed of a Mo deposition layer and a Mo diffusion layer (Fig. 12).

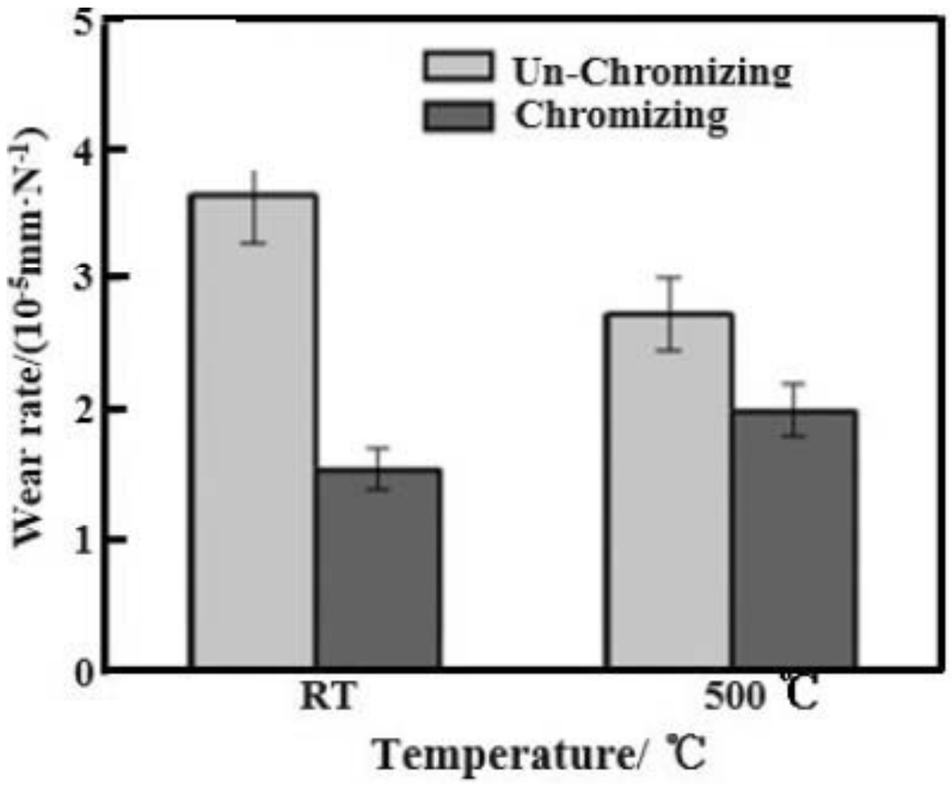

Fig. 11. Mass losses of chromized layer and Ti_2AlNb after wearing under room temperature and 500 °C.

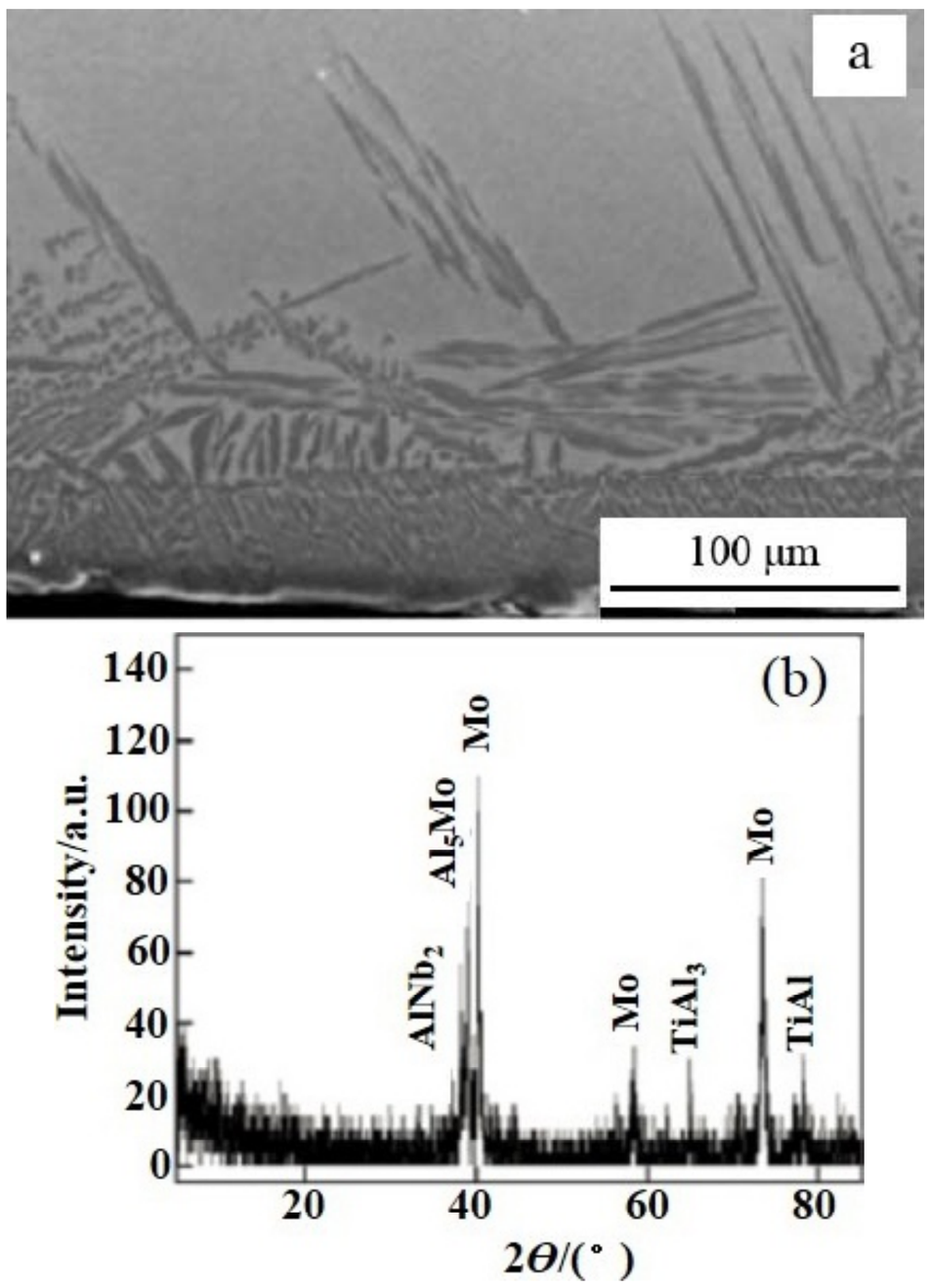

Fig. 12. Cross-sectional microstructure (a), composition profile (b) and XRD pattern of (c) molybdenizing layer on Ti_2AlNb.

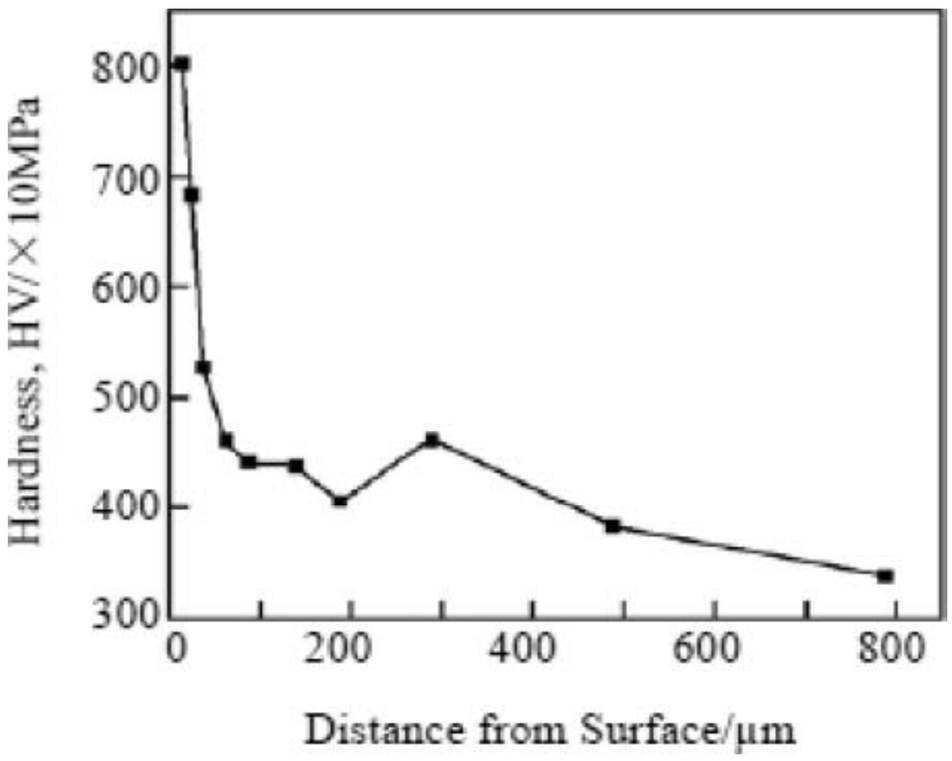

Fig. 13. Microhardness profile of molybdenizing layer on Ti_2AlNb.

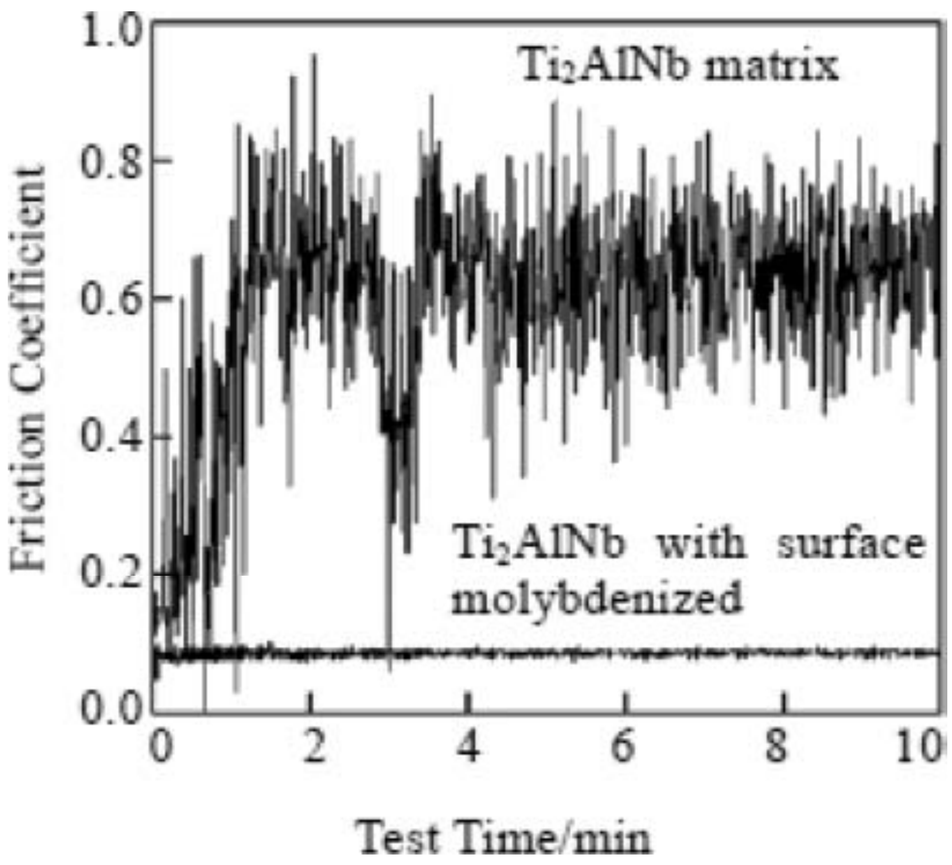

Fig. 14. Coefficients of friction of molybdenizing layer and Ti_2AlNb.

The surface hardness of Ti_2AlNb alloy was enhanced remarkably through DGPSA molybdenizing (Fig. 13). The tribological property of Ti_2AlNb was greatly enhanced after DGPSA molybdenizing, which was revealed by lower friction coefficient and narrower wear scar as presented in Figs. 14 and 15.

Liu et al. [84] prepared hard molybdenizing layer on the surface of g-TiAl alloy by DGPSA. The molybdenizing layer indicated lower coefficient of friction and mass loss than those of γ-TiAl alloy in pin-on-disk wear tests. The molybdenizing layer had remarkable improved the wear resistance of γ-TiAl alloy.

Xu et al. [85,86] obtained molybdenizing layer on γ-TiAl alloy by DGPSA. Due to the formation of a compact Ti-Al-Mo alloyed layer on the surface of γ-TiAl alloy, the alloyed layer provided excellent protection of γ-TiAl alloy substrate, and the treated γ-TiAl alloy showed more promising high-temperature oxidation resistance.

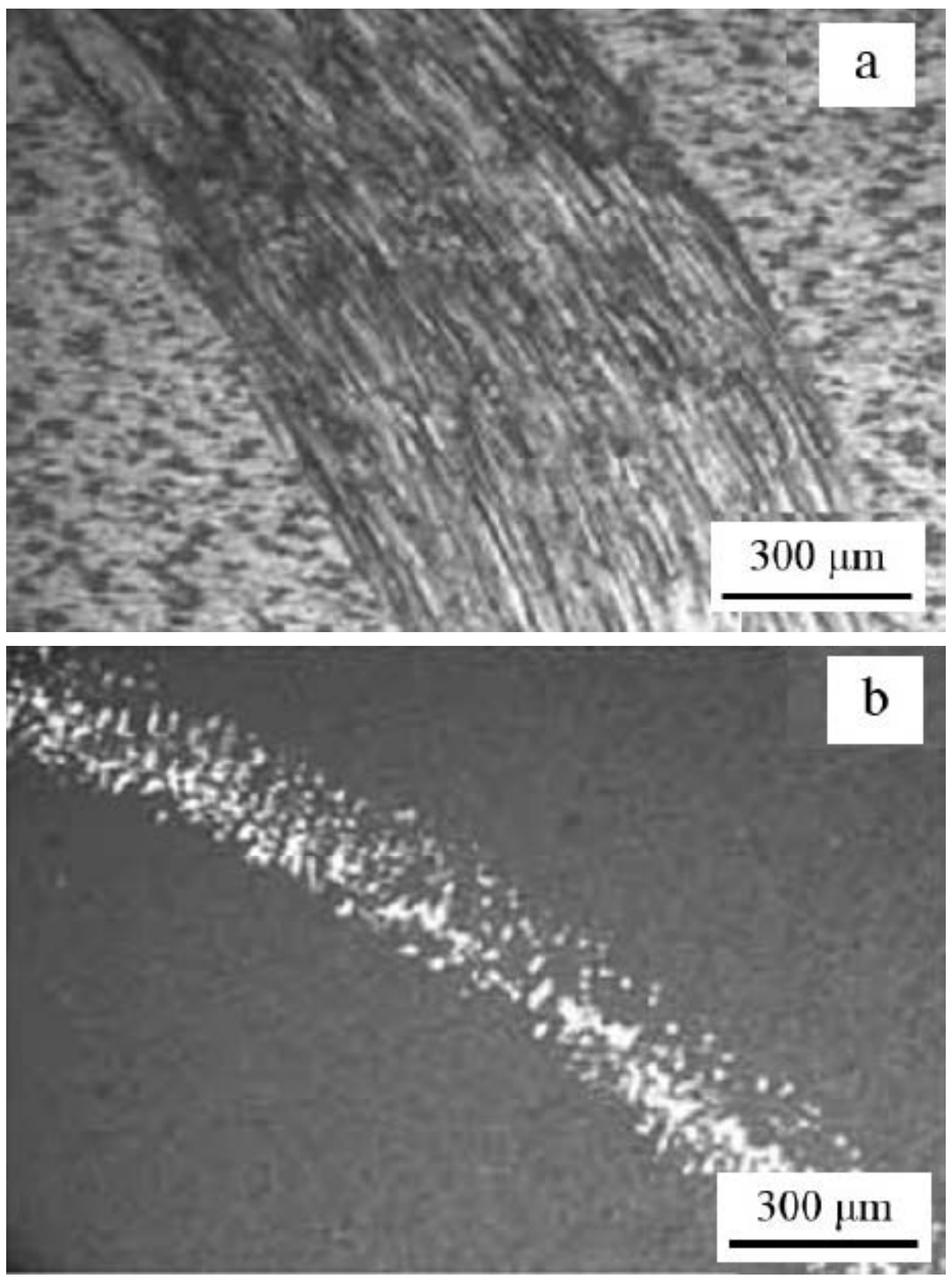

Fig. 15. Wear scars of Ti_2AlNb (a) and molybdenizing layer (b).

Guo et al. [87] performed DGPSA niobizing on γ-TiAl alloy. The effects of alloying temperature and time on the element content and the thickness of the alloyed layer were studied. The results showed that the thickness and composition of the alloyed layer were closely related to alloying temperature and time. A deposit layer on the surface of γ-TiAl was formed resulting from both too low alloying temperature and too long alloying time. The appropriate thickness and composition distribution of the alloyed layer was made by an optimized process parameter of 1100 °C for 3 h was useful to improve the wear and oxidation resistances.

Zheng et al. [88] investigated oxidation behaviors of DGPSA niobized γ-TiAl alloy. The diffusion layers were formed on γ-TiAl substrates by DGPSA niobizing process. The TiAl substrates and niobized γ-TiAl specimens were oxidized in static air for 360 ks at 1223 and 1323K. The interrupted-oxidation kinetics curves of bare γ-TiAl were approximately straight lines. In contrast, the mass of all the niobized specimens increased in accordance with logarithmic law (Fig. 16). The oxidation rate of DGPSA niobized γ-TiAl in steady stage decreases by more than one order of magnitude. The scale was basically composed of four layers from the surface inward of γ-TiAl substrate, and pores and a gap which resulted in the spallation of the scale were obvious.

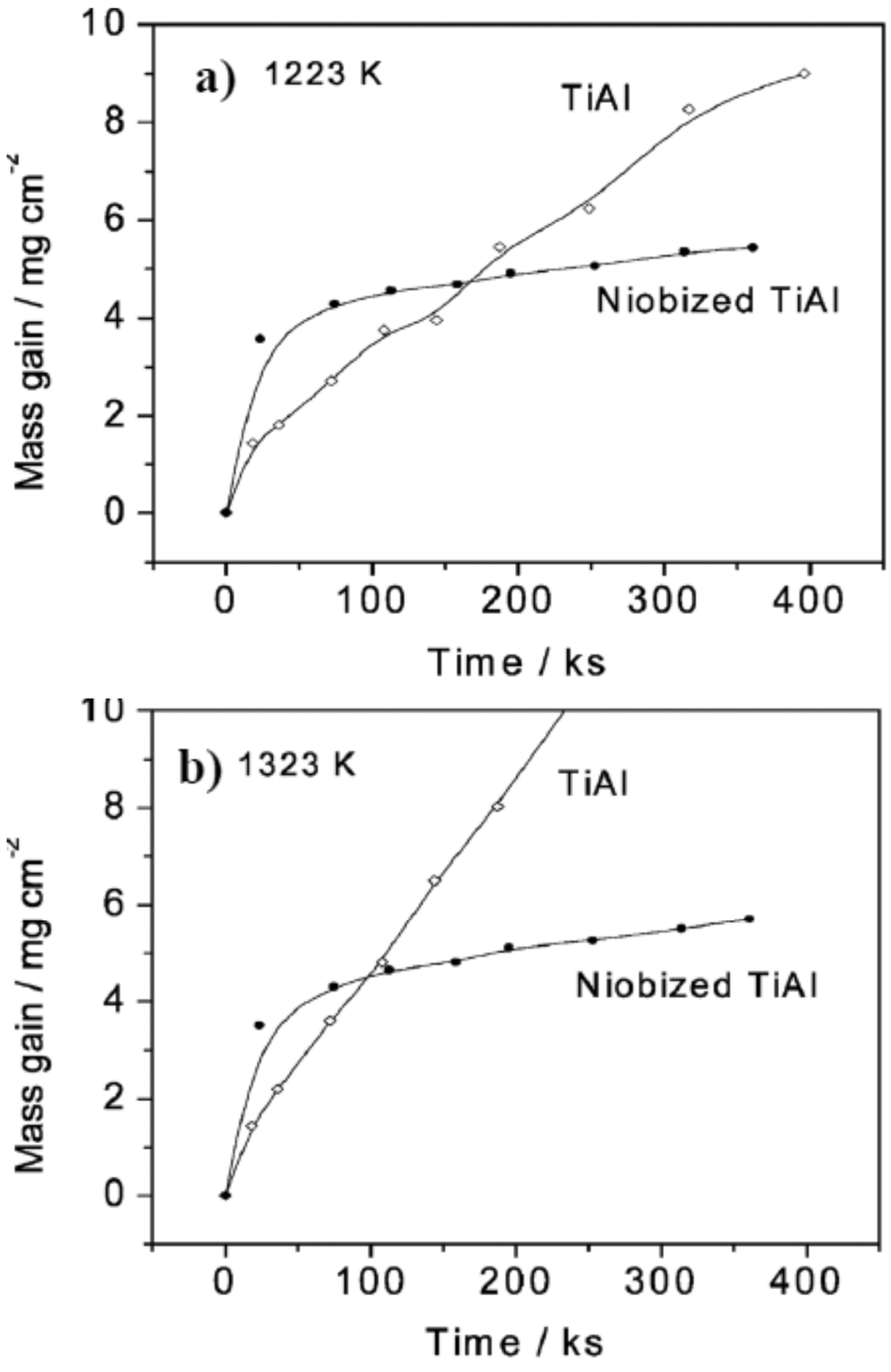

Fig. 16. Interrupted-oxidation kinetics of niobized TiAl and untreated TiAl (a) 1223K; (b) 1323K.

However a uniform and adherent Al_2O_3 layer formed on the niobized γ-TiAl can be an obstacle prohibiting oxygen from diffusing inwards, which provides excellent protection for the substrate at 1223K (Fig. 17). The DGPSA niobizing had remarkably improved the oxidation resistance of γ-TiAl.

Chen et al. [89] obtained niobizing layer on γ-TiAl alloy via DGPSA (Fig. 18) and studied the oxidation behaviors of niobized g-TiAl alloy and its parent sample. It was indicated that the diffusion layer formed on γ-TiAl substrate presented better oxidation resistance than that of untreated γ-TiAl. The role of Nb for improving the oxidation resistance of treated γ-TiAl was considered to be achieved by strengthening the activity of Al, which was induced by the DGPSA niobizing process.

Liu et al. [90] applied DGPSA to produce a niobizing layer on γ-TiAl alloy in order to improve its oxidation and wear resistance. The results showed that a Nb-alloyed layer, with a thickness of 12 μm was formed on γ-TiAl alloy (Fig. 19a). Seen from its composition distribution, the alloyed layer contained a high Nb-concentration region (marked as A in Fig. 19b) and a diffusion region between zone A and the substrate. From the outside-in compositions, the

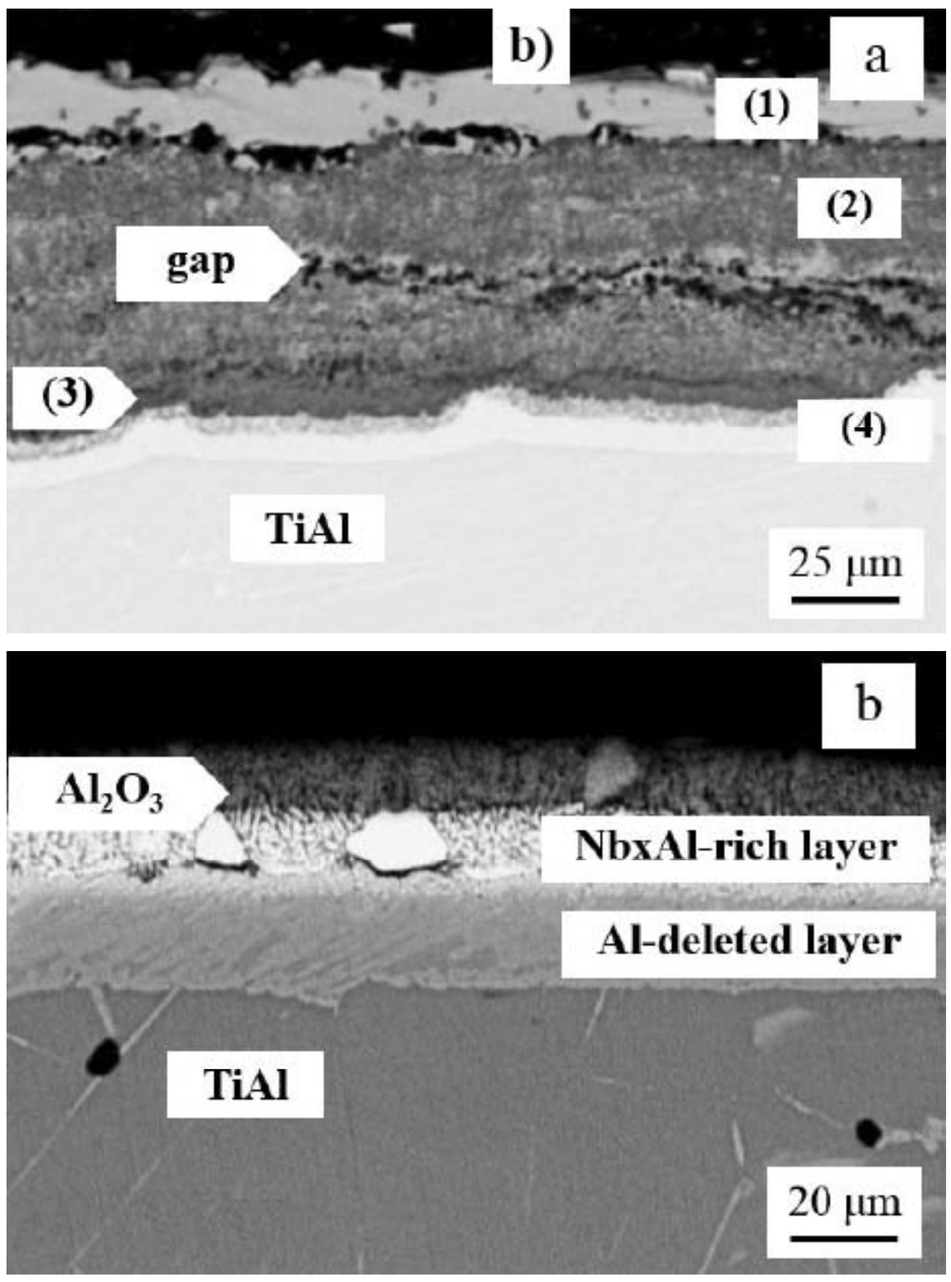

Fig. 17. Cross-sectional microstructures of scales after 360-ks oxidation at 1223: (a) TiAl: (1) TiO_2, (2) TiO_2+Al_2O_3, (3) Al_2O_3-rich layer, (4) Al-depleted layer; (b) niobized TiAl.

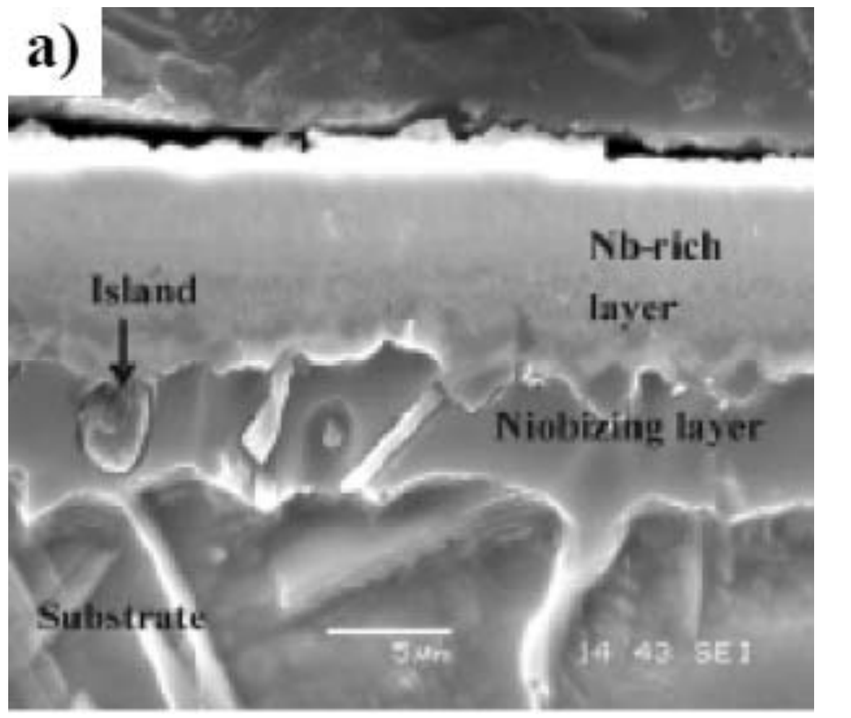

Fig. 18. Cross-sectional microstructure (a) and XRD pattern (b) of niobized TiAl alloy.

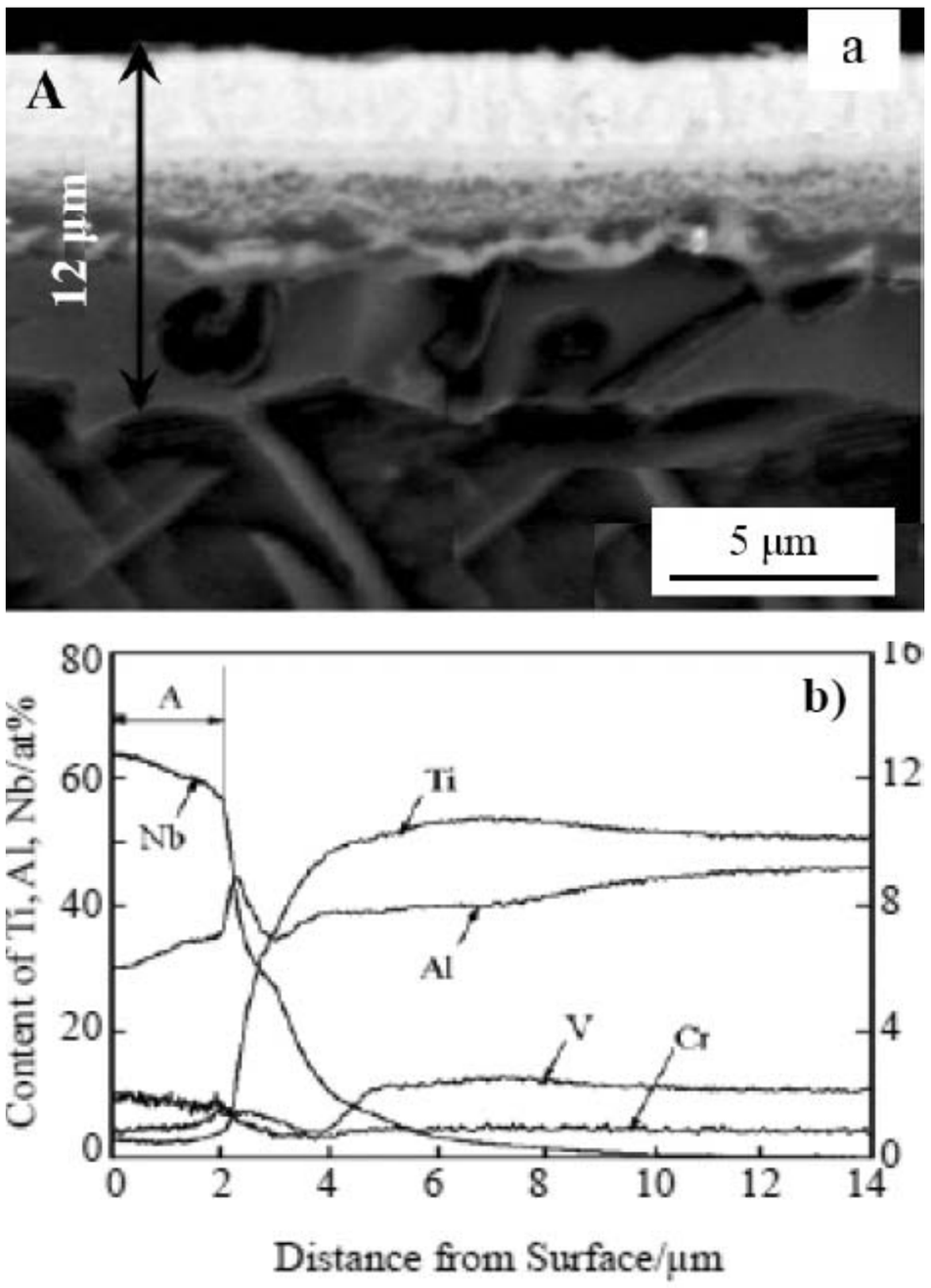

Fig. 19. Cross sectional morphology (a) and composition distribution (b) of Nb-alloyed layer.

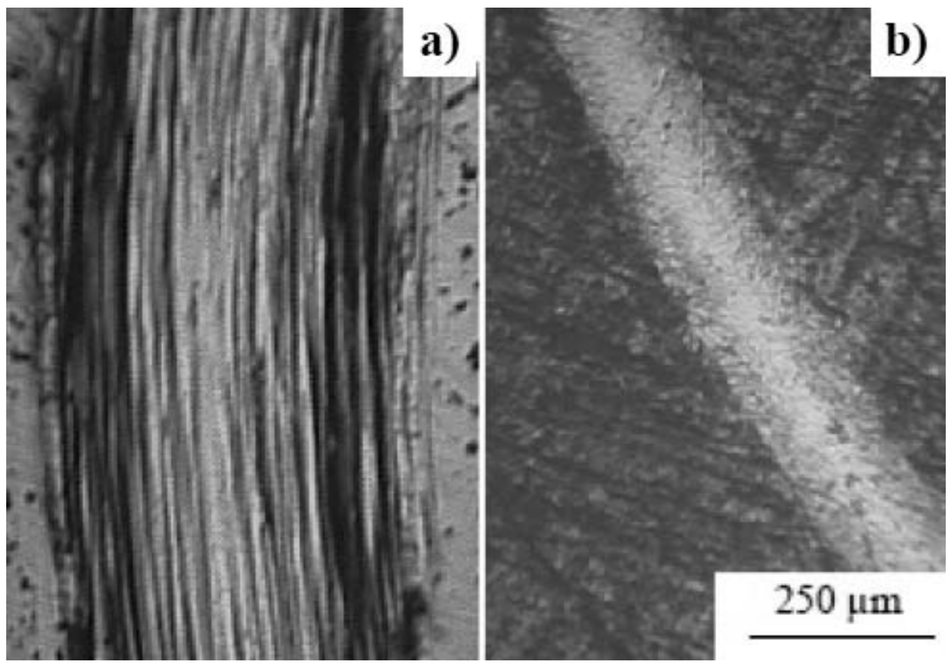

Fig. 20. Worn surface of TiAl (a) and TiAl-Nb (b) against ASTM W1-111/2 steel.

alloyed layer could be divided into regions of niobium-rich/aluminum-rich/titanium-rich/substrate. The alloyed layer consisted of $AlNb_2$, $AlNb_3$, Ti_2AlNb and pure niobium was compact and homogeneous. Under dry sliding conditions, the wear resistance of niobizing layer at ambient temperature and 600 °C were better than those of untreated γ-TiAl alloy indicating by wear scars (Figs. 20 and 21).

Wu et al. [91,92] performed tungstenizing on Ti-Al-Nb substrate using DGPSA. The formed tungstenized layer was comprised of three distinct sub-layers namely sediment layer, transition layer and diffusion layer, with a total layer thickness of over 25 μm. The concentration of the tungsten decreased gradually as the layer depth increased (Fig. 22). The continuous change in the tungsten content affected the mechanical properties of the alloyed layer. Both surface micro-hardness and elastic modulus of plasma alloyed surface gradually decreased with the increase of indentation depth,

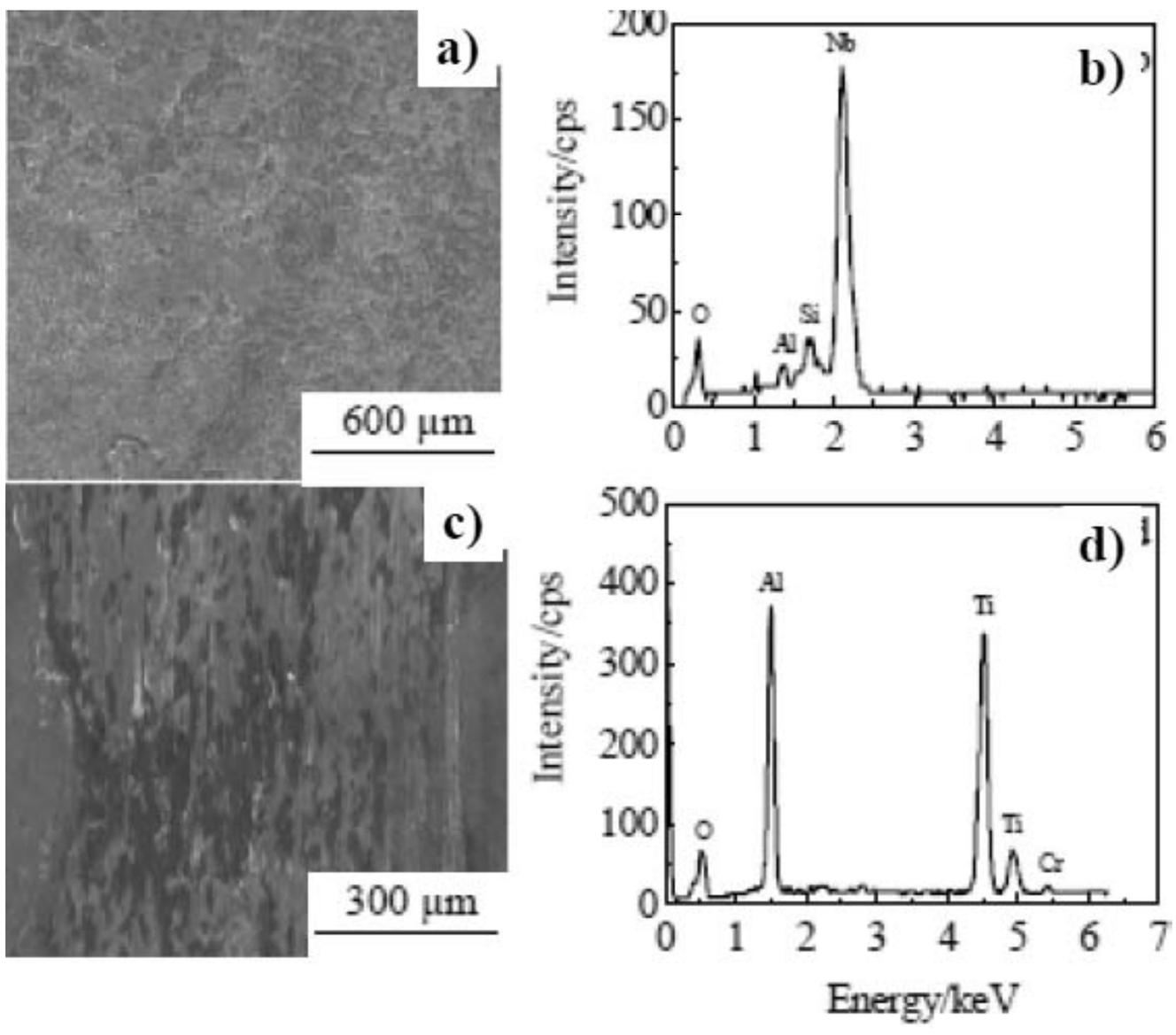

Fig. 21. SEM images and EDS compositions of worn scars of TiAl-Nb (a, b) and TiAl (c, d) at 600 °C.

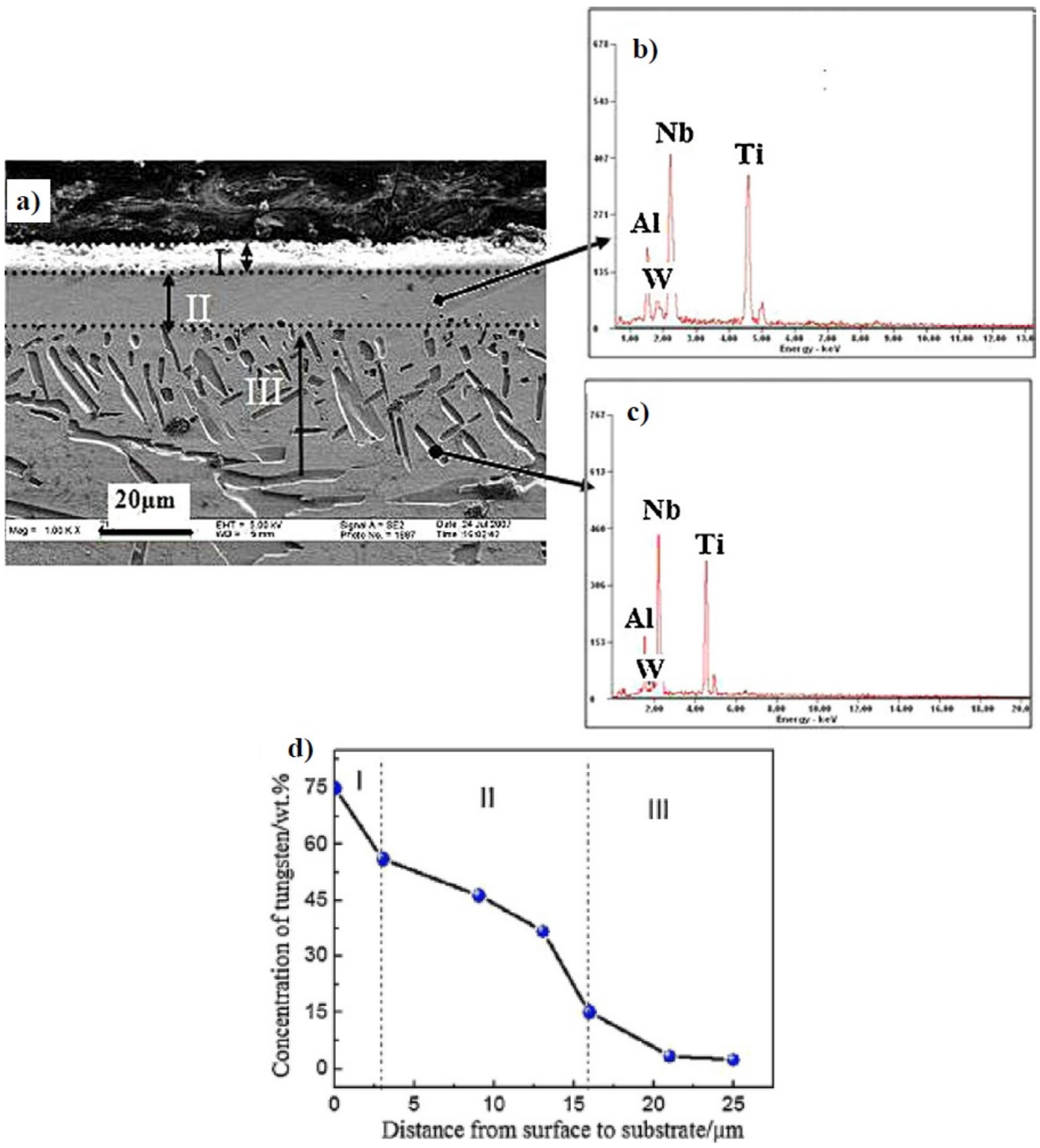

Fig. 22. Cross-section morphology of the tungstenized layer (a) and the corresponding EDS analyses of (b) the transition layer and (c) the diffusion layer, (d) concentration distribution of tungsten.

most probably because of the three different regions in the alloyed layer. As for the mechanical properties, the tungstenized layer exhibited significantly higher dynamic micro-hardness and elastic modulus than the substrate.

3.2. DGPSA with binary elements

Wu et al. [80] performed a two-step duplex treatment on Ti-Al-Nb alloy, chromizing followed by carburizing via DGPSA. Dry sliding friction tests on the Ti-Al-Nb alloy substrate, the chromized layer, and the duplex-treated layer were completed by ball-on-disk tribometer at room temperature using Si_3N_4 balls counterface materials. The results indicated that the duplex-treated layer was mainly composed of $Cr_{23}C_6$, Cr_2Nb, pure chromium, and carbon phases. The ultra-microhardness of the duplex-treated layer was higher than that of the chromized layer, whereas the elastic modulus of the duplex-treated layer was lower than that of the chromized layer. The friction coefficient of the duplex treated layer was about three times lower than that of the chromized layer, while the wear rate was one order of magnitude lower than that of the chromized layer. Cr-C DGPSA duplex treatment was considered as an effective method to improve the tribological performance of Ti-Al-Nb alloy.

Li et al. [93-96] achieved Cr-Si co-alloying on γ-TiAl alloy was by using DGPSA. The concentration of Cr and Si displayed gradient distribution from the surface to the inside. The Cr-Si layer was composed of Al_xCr_y, Cr_xSi_y, Ti_xCr_y, and Ti_xSi_y phases. The surface microhardness had reached HV 1000. Dense CrO_2 and continuous Al_2O_3 film, which provided promising protection against oxidation, were formed in the process of oxidation. The Cr-Si co-alloying layer had significantly improved the wear resistance of γ-TiAl alloy. The Ti_xSi_y ceramic phase, tough transition layer and high Si content in the Cr-Si layer contributed to wear resistance promotion.

Liu et al. [84] fabricated Mo-C alloying layer, molybdenizing followed by carburizing via employ of DGPSA. The surface layer on γ-TiAl alloy obtained

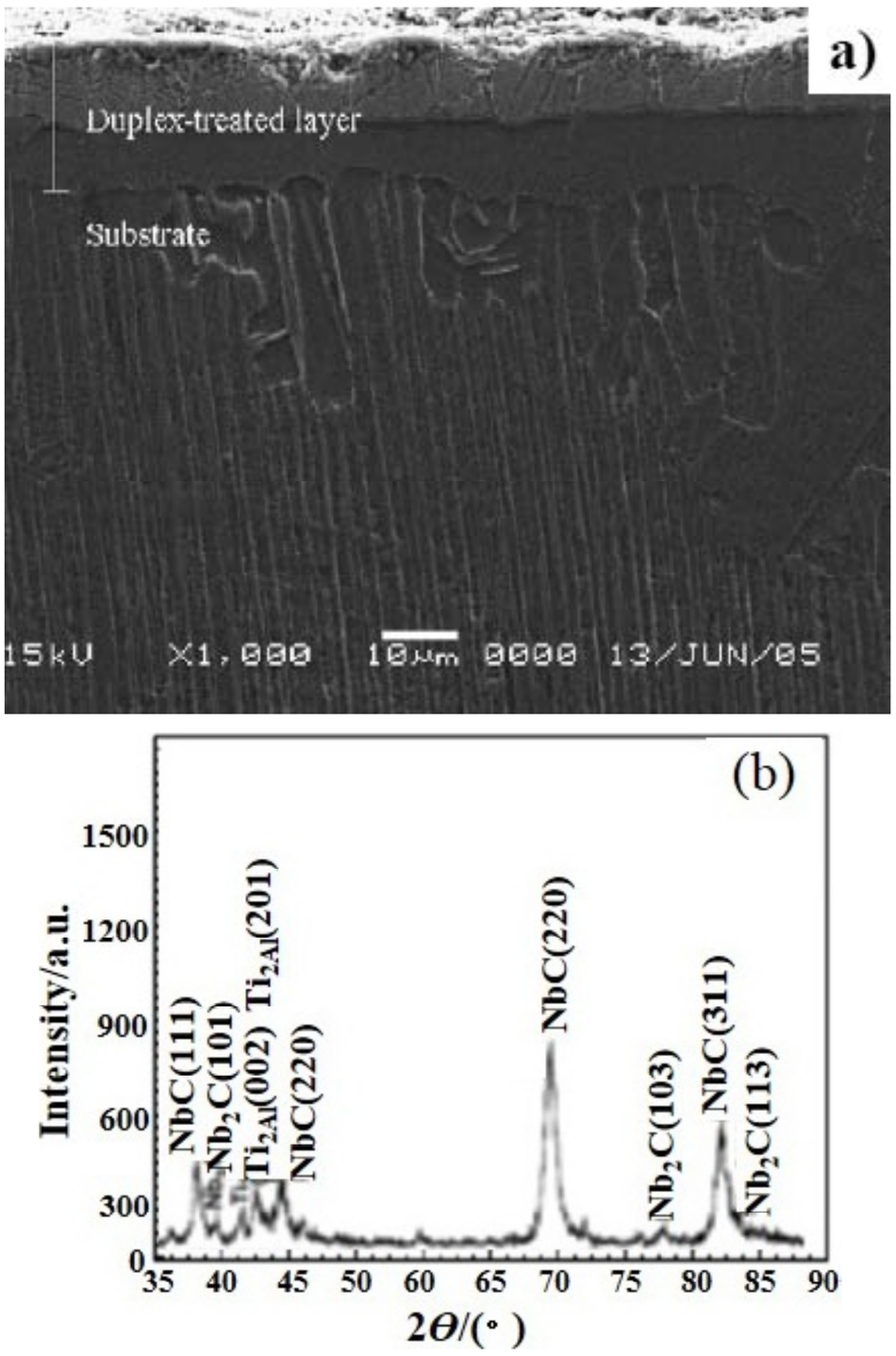

Fig. 23. Cross-sectional microstructure (a) and XRD pattern (b) of Nb-C layer on γ-TiAl.

by carburizing at 1000 °C following molybdenizing at 1125 °C consisted of a hard layer with a thickness of 20 μm and showed a gradient distribution in chemical composition. The hard phases on γ-TiAl with an average hardness more than HK 890 were identified as MoC and Mo_2C. The pin-on-disk wear tests showed that the Mo-C alloying layer had improved the wear resistance of γ-TiAl alloy. Meanwhile, it was found that duplex treatment of molybdenizing followed by carburizing via employ of DGPSA can improve the friction coefficient of γ-TiAl more effectively than that only by carburization.

Ben et al. [97] investigated the Nb-C co-alloying on γ-TiAl alloy applying DGPSA. It was seen that when the difference between the source voltage and work piece was 250 V, a thick and compact Nb-C layer could be formed at 1000 °C for 3h with a distance between the source electrode and work piece of 18 mm and gas pressure 25 Pa. The surface hardness of the obtained Nb-C layer reached HV 1150.

Xing et al. [98] used the DGPSA to prepare a Nb-C layer on γ-TiAl alloy. It was confirmed that the Nb-C layer showed a better combination between wear and oxidation resistance. The first-principle method was applied to study the diffusion of C atoms and Nb atoms on γ-TiAl (010) surface. By analyzing final energy and forming enthalpy, it was found that the DGPSA of Nb-C had made the final energy of the γ-TiAl (010) surface cell enhanced, but decreased its forming enthalpy, therefore the stability of the cell was improved.

Liu et al. [99] prepared Nb-C layer on γ-TiAl alloy by a duplex treatment using DGPSA in order to improve the tribological property of γ-TiAl alloy. As shown in Fig. 23, the obtained layer was continuous and compact; it was composed of Nb-carbides. After dry sliding against high carbon steel counterpart, the results showed that the Nb-C alloyed γ-TiAl had a lower coefficient of friction and a lower wear volume. The surface hardening effect by the existence of NbC and Nb_2C carbides and excessive carbon, as well as thicker layer with a gradient distribution of hardness were the main contribution to the tribological performance of γ-TiAl.

Guo et al. [100] discussed oxidation resistance of DGPSA Nb-C alloyed γ-TiAl alloy. The obtained Nb-C alloyed surface was uniform and compact; it was composed of NbC and Nb_2C which could enhance the wear resistance of γ-TiAl (Fig. 24). After the cyclic-oxidation tests in static air at 900 °C for 10^3 h. The Nb-C alloyed TiAl showed better oxidation resistance in comparison with γ-TiAl alloys. Moreover, the oxide scale of Nb-C alloyed TiAl exhibited better spallation resistance than the untreated γ-TiAl. After oxidation, more Al_2O_3 and nitrides were formed on the surface of the Nb-C alloyed γ-TiAl. The coexistence niobium and carbon could lead to the formation of a compact oxide layer with more Al_2O_3 on the surface, which offered better oxidation resistance.

By using DGPSA, Wang et al. [101, 102] obtained a Nb-C layer on γ-TiAl alloy. It was found that the addition of Nb and C could promote the growth of Al_2O_3 and significantly improve the oxidation resistance of γ-TiAl alloy. Meanwhile the Nb-C layer showed excellent corrosion resistance by its chemical stable and mechanical isolation effects.

Wu et al. [103] performed W-C duplex treatment on the Ti_2AlNb alloy by using DGPSA process to enhance its wear resistance. The microstructure and high-temperature tribological behaviors of the untreated and W-C duplex treated samples were investigated. The results showed that the duplex treated layer was mainly composed of W_2C or $W_6C_{2.54}$ phases. The contents of W and C elements in the alloyed layer gradually distributed along the depth of the W-C layer. The diffusion depth of W is about 12 μm, while the carbon atoms most exist in

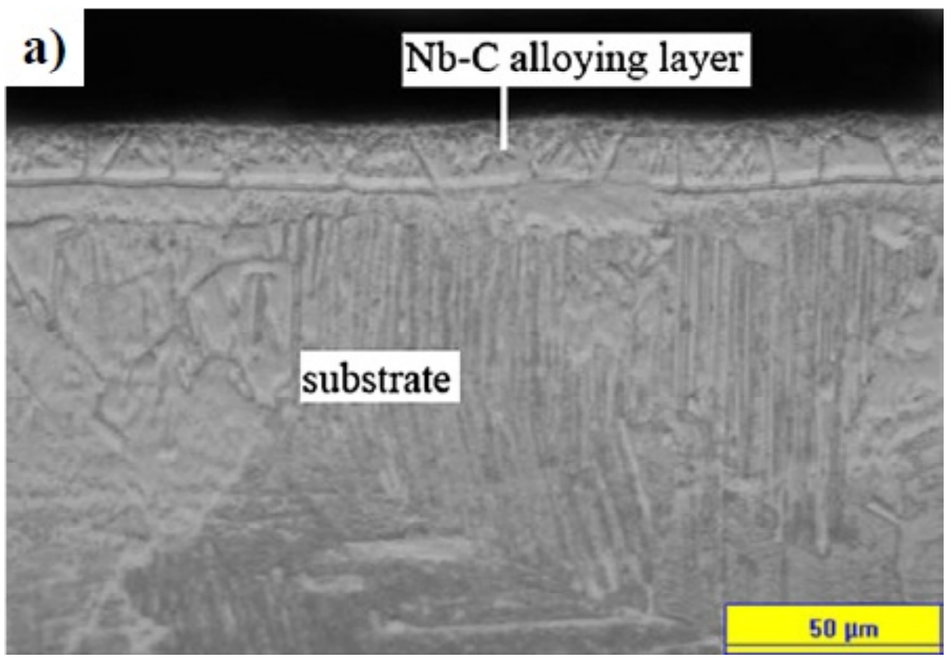

Fig. 24. Cross-sectional microstructure (a) and XRD pattern (b) of Nb-C layer on γ-TiAl.

the depth more than 12 μm. High-temperature tribometer tests indicated that the friction coefficient of the W-C duplex treated layer was approximately 1/6 that of the Ti_2AlNb alloy substrate. The wear rate of the duplex treated layer was about 28 % that of the untreated one. The W-C duplex treatment had obviously improved the high-temperature tribological performance of Ti_2AlNb alloy.

Zheng et al. [104] applied the DGPSA technique to realize the W-C co-alloying of γ-TiAl alloy. The optimization of process parameters of metallic cementation: Work pressure for 50~55 Pa, the source voltage is 1000 V, spacing of the electrodes between 16~20 mm and heat preservation time is 4 h, choosing a temperature of 1000 °C. The results showed that W-C composite alloying layer had enhanced the wear resistance of γ-TiAl at room temperature and 500 °C, especially the increase of W-C composite alloying layer at 500 °C is particularly evident.

Wei et al. [105,106] prepared Cr-W alloying layer on γ-TiAl alloy via DGPSA. As shown in Fig. 25, the Cr-W alloying layer was smooth and uniform, the alloying layer closely bonded to the matrix without defects. The Cr-W alloying layer was composed of AlTi, Al_5W, W, Cr and Cr_2Ti (Fig. 26). Cr-W alloying

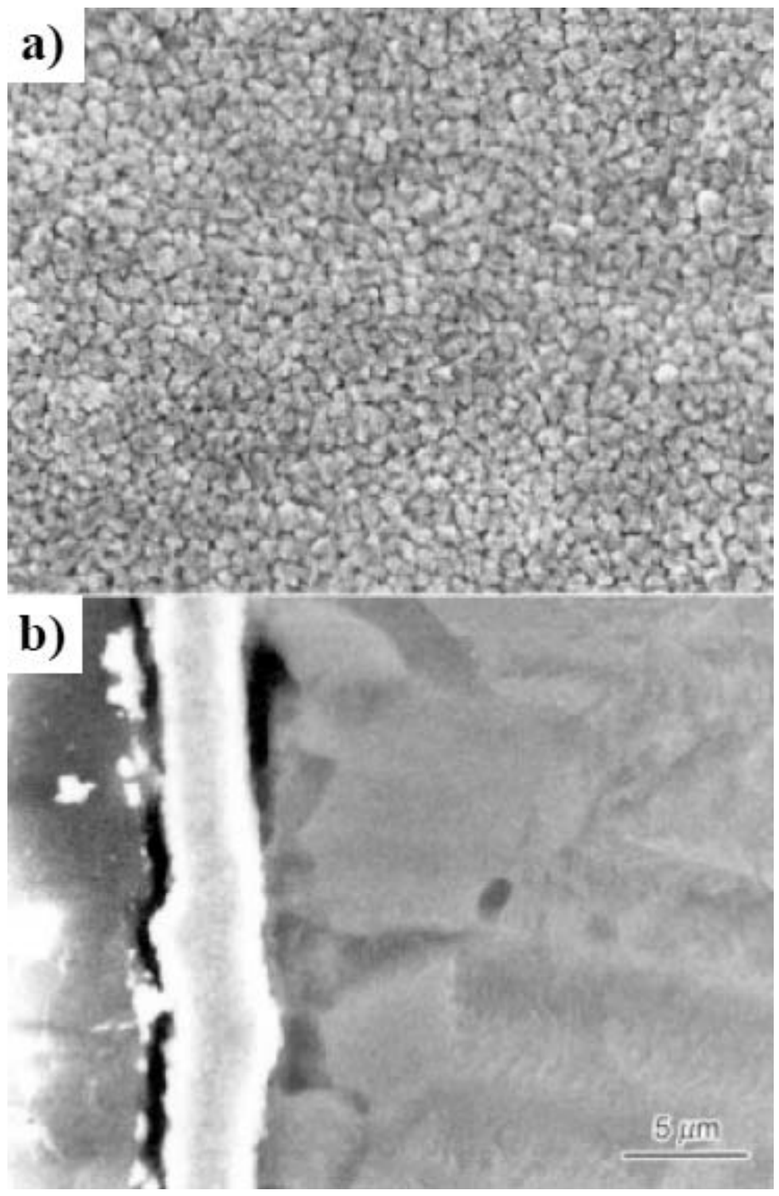

Fig. 25. Surface morphology and cross-sectional microstructure of Cr-W layer.

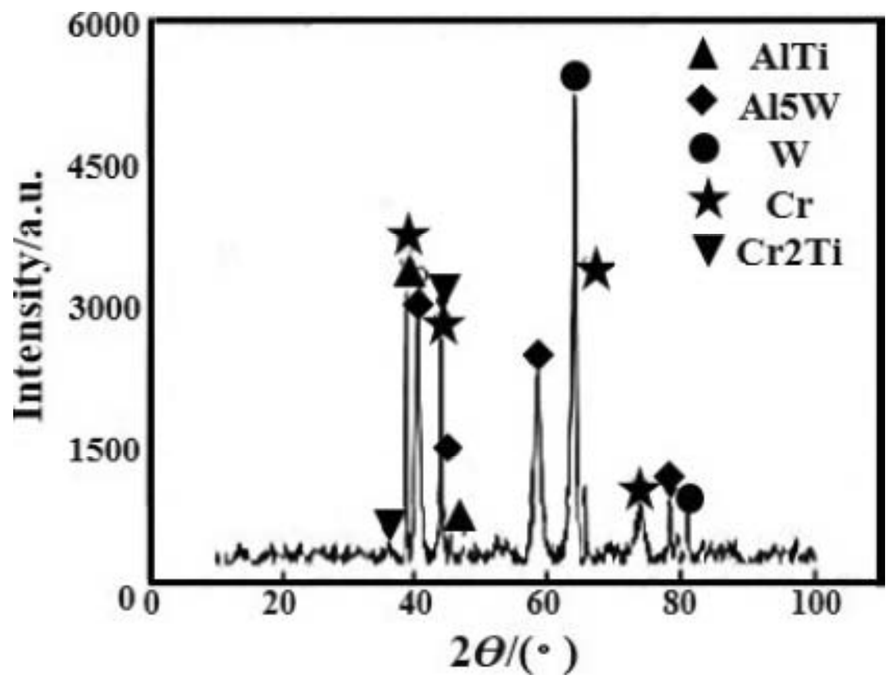

Fig. 26. XRD pattern of Cr-W layer on γ-TiAl.

by DGPSA had greatly improved the oxidation resistance of γ-TiAl alloy at different temperatures. The Cr-W alloying layer indicated higher hardness than that of the matrix. Meanwhile the Cr-W alloying layer showed obviously improved wear resistance at ambient temperature and 600 °C comparing with untreated γ-TiAl alloy indicating by wear scars (Figs. 27 and 28).

Fan et al. [107] studied Ni-Cr alloying on γ-TiAl surface by DGPSA process to improve its oxidation resistance and wear resistance. The research results showed that after oxidation in air at 900 °C for 100 h, dense oxide film consisted of Al_2O_3, TiO_2, Cr_2O_3, and $NiCr_2O_4$ had formed on the surface of the Ni-Cr alloyed sample. The oxide film closely bonded

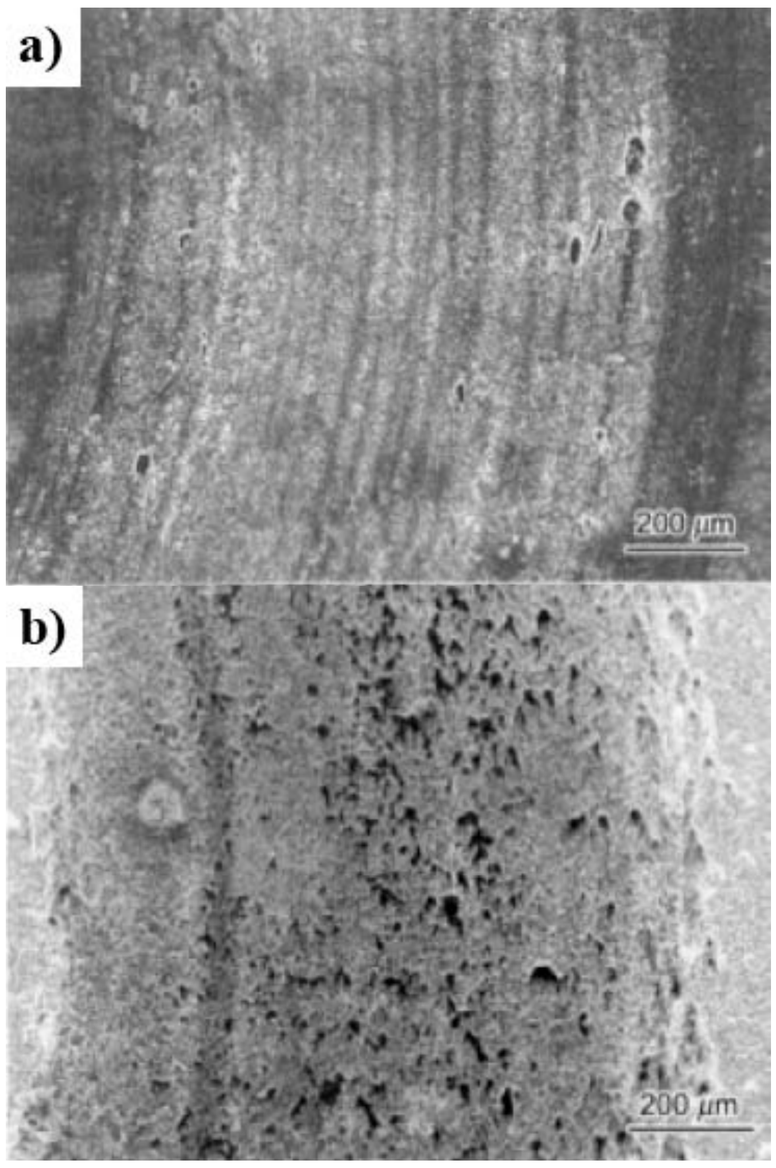

Fig. 27. Wear scars of γ-TiAl (a) and Cr-W layer (b) wearing under room temperature.

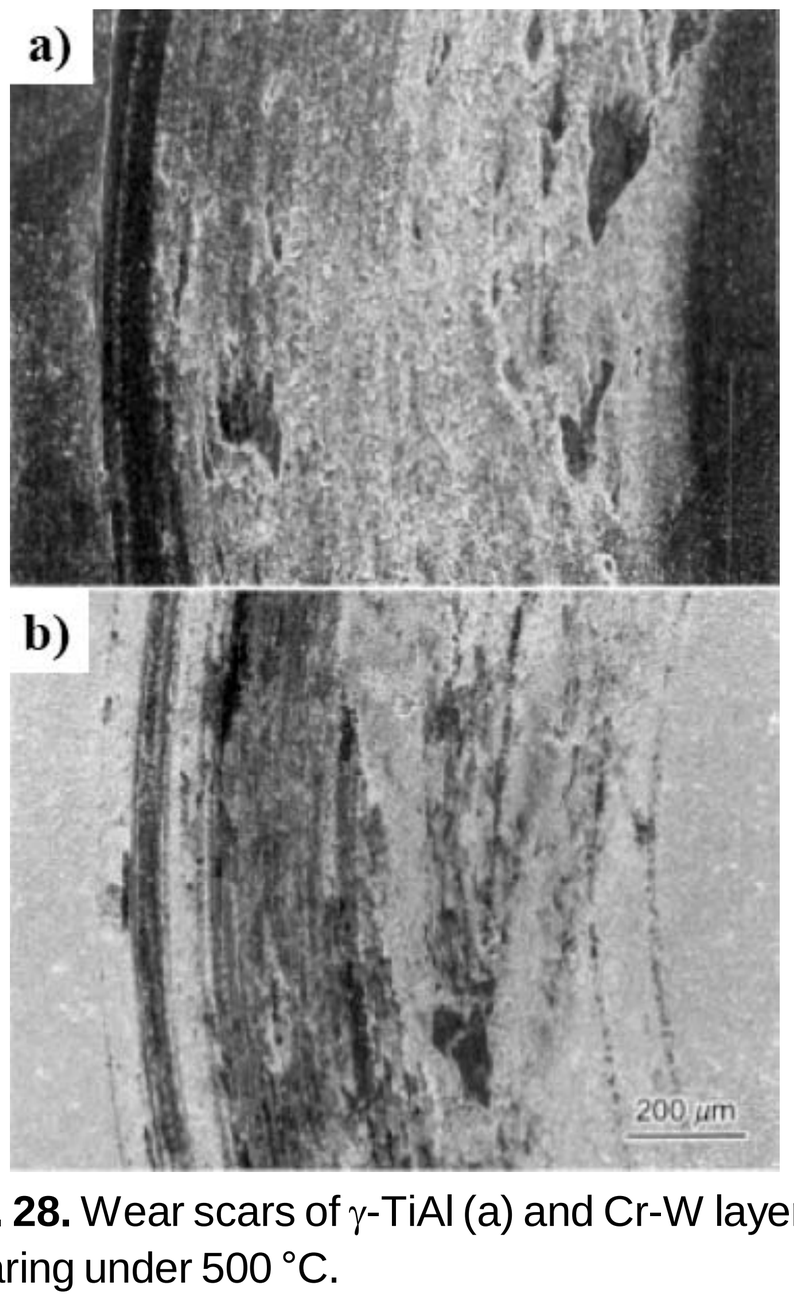

Fig. 28. Wear scars of γ-TiAl (a) and Cr-W layer (b) wearing under 500 °C.

to the beneath layer and had good oxidation resistance. The oxide film on TiAl substrate was loose and revealed poor oxidation resistance. Under high temperature wearing tests, Ni-Cr alloying layer showed a lower friction coefficient and mass loss, which meant the wear resistance of γ-TiAl alloy had been improved by Ni-Cr alloying treatment. Ni-Cr

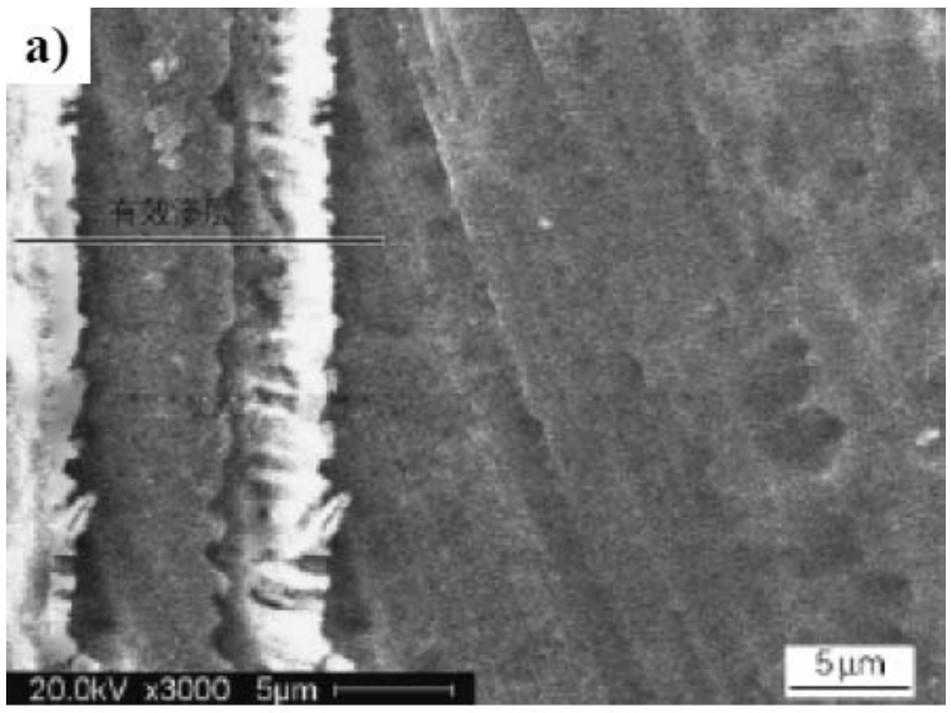

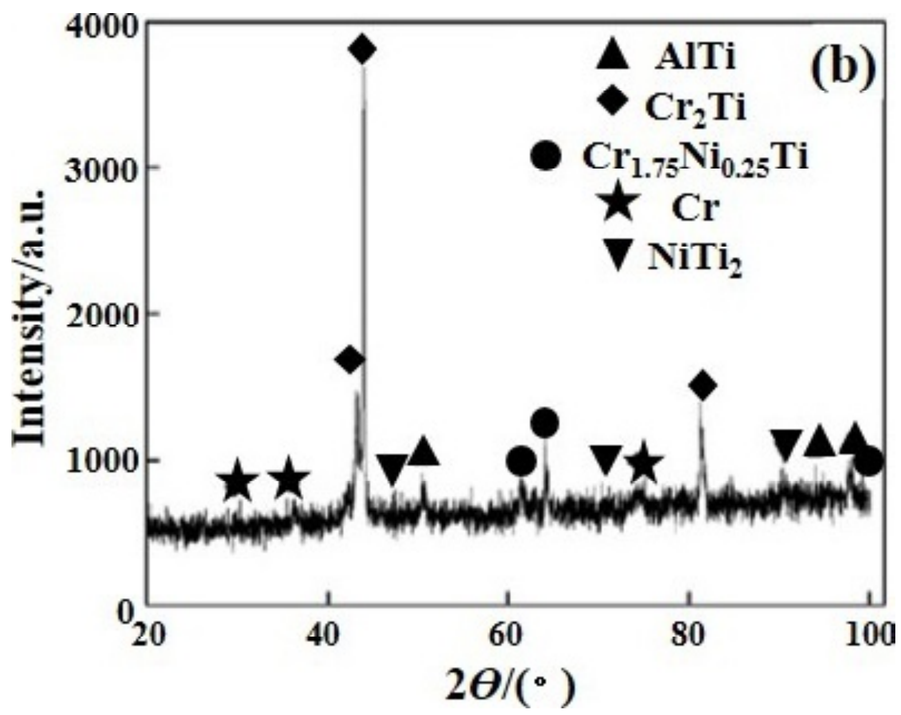

Fig. 29. Cross-sectional microstructure (a) and XRD pattern (b) of Ni-Cr layer on γ-TiAl.

alloying layer indicated no obvious friction-reduction effect in fretting wear, but improved the fretting wear resistance.

Huang et al. [108] also prepared Ni-Cr alloying layer on γ-TiAl alloy surface by DGPSA. The results showed that the diffusion thickness of alloying layer is about 25 μm, and the phase constitution of the Ni-Cr layer was Cr_2Ti, AlTi, Cr, $NiTi_2$, and $Cr_{1.75}Ni_{0.25}Ti$ (Fig. 29). The contents of Ni and Cr in the alloying layer decreased gradually from surface to substrate. The alloying layer and the matrix were tightly bonded. The hard Ni-Cr layer showed better tribological properties than those of γ-TiAl alloy matrix at room temperature (Fig. 30) and at 773K (Fig. 31).

In Wu et al.'s work [109]; the Ti_2AlNb based alloys were chromium-tungstened (Cr-W) and nickel-chromized (Ni-Cr) by the DGPSA process to improve their high temperature oxidation resistance. After exposing at 1093K, the TiO_2 layer was formed on the bare alloy and accompanied by the occurrence of crack, which promoted oxidation rate. The oxidation behaviors of Ti_2AlNb-based alloys were improved by surface alloying due to the formation of protective Al_2O_3 scale on Cr-W layer or continuous and dense $NiCr_2O_4$ film on Ni-Cr layer. The alloyed

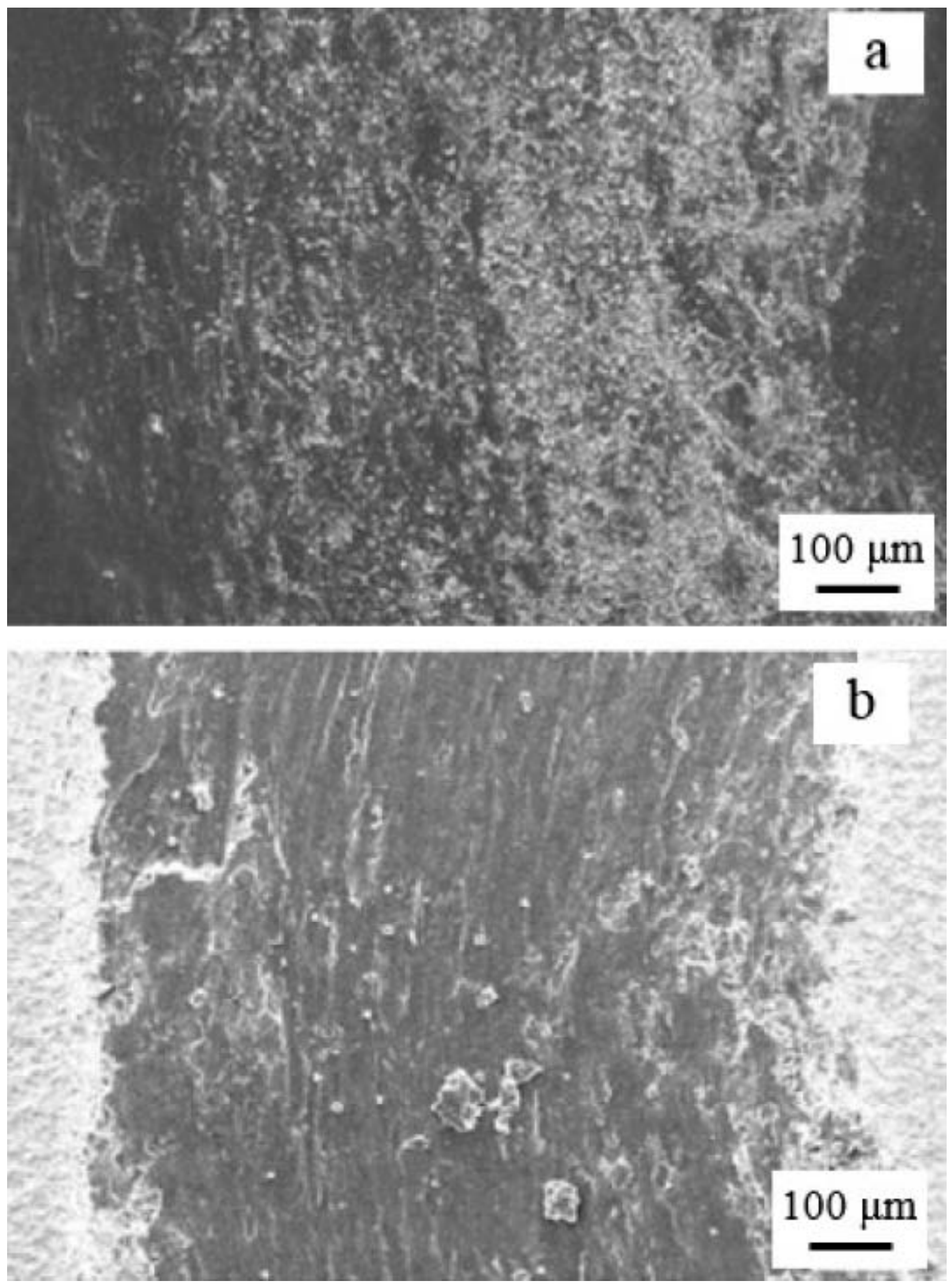

Fig. 30. Wear scars of γ-TiAl (a) and Ni-Cr layer (b) at room temperature.

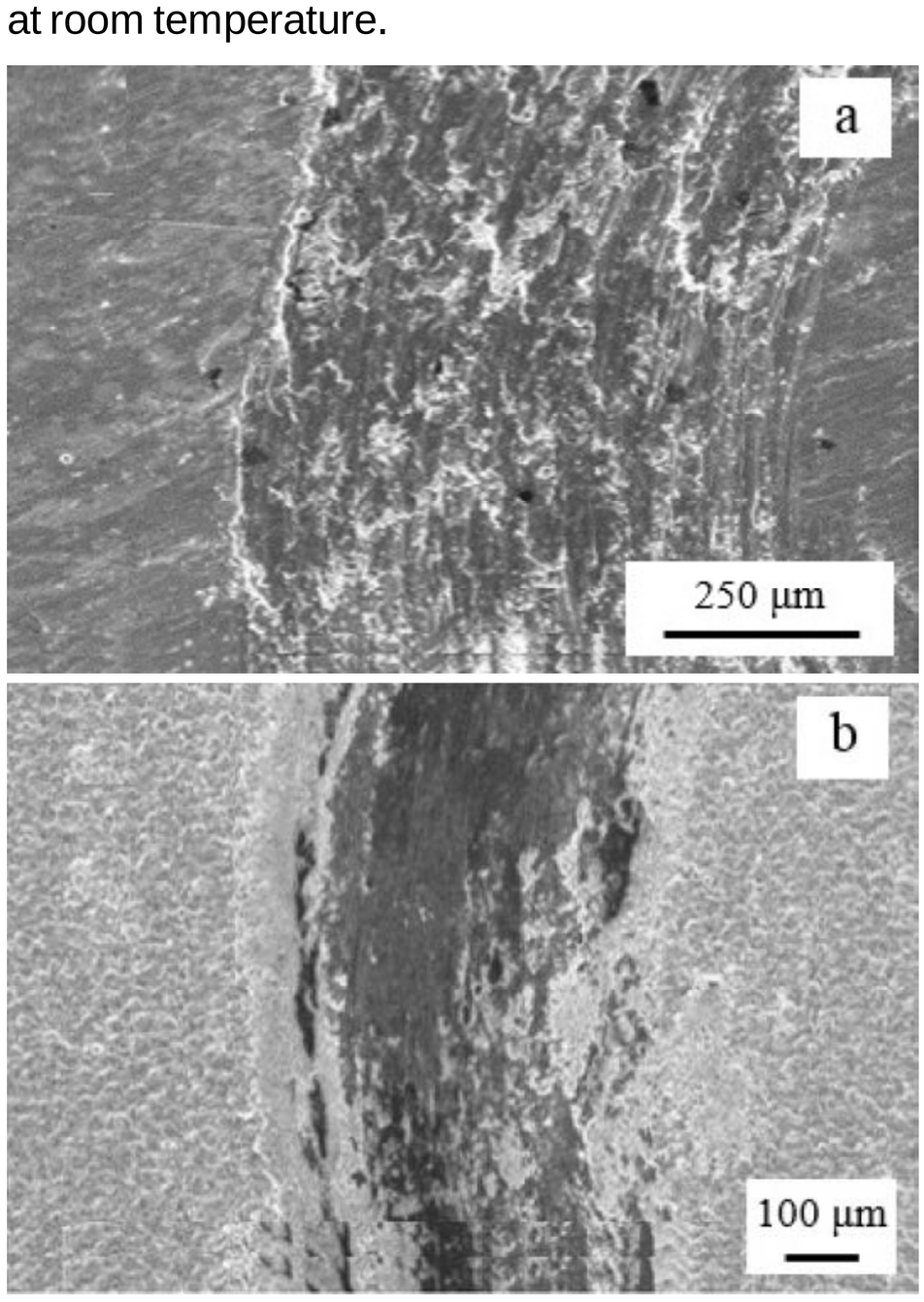

Fig. 31. Wear scars of γ-TiAl (a) and Ni-Cr layer (b) at 773K.

layers exhibited superior scale spallation resistance than that of the Ti_2AlNb-based alloy. The Ni-Cr alloyed layer presented better high-temperature oxidation resistance than Cr-W layer.

3.3. DGPSA with multi-elements

Huang et al. [110] used the DGPSA technique to improve tribological properties γ-TiAl alloy and high-temperature oxidation resistance by forming NiCr-O composite alloying coating. Fig. 32 presented that the NiCr-O composite alloying was smooth and compact; the uniform and continuous alloying coating could be divided into four layers and closely bonded to the substrate. NiCr-O composite alloy-

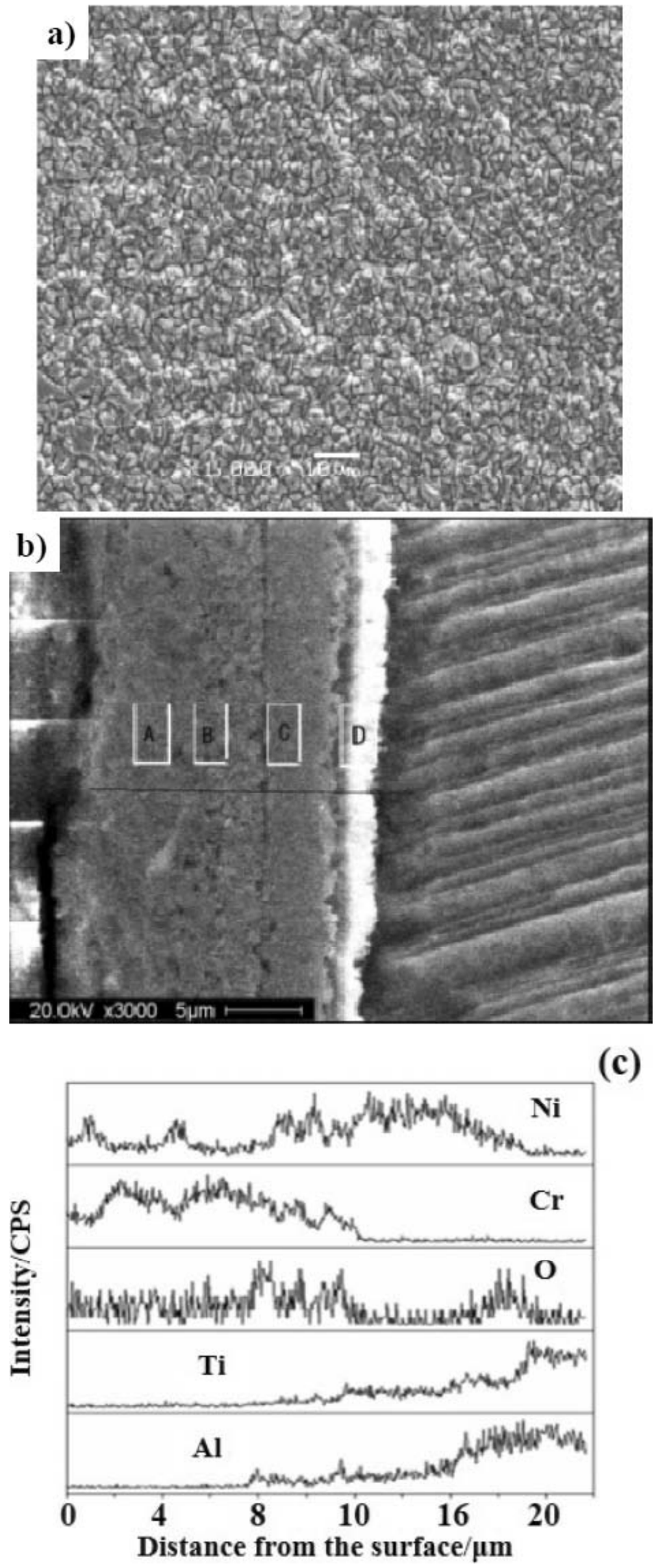

Fig. 32. Surface morphology (a), cross-sectional microstructure (b) and composition distribution (c) of NiCr-O duplex layer.

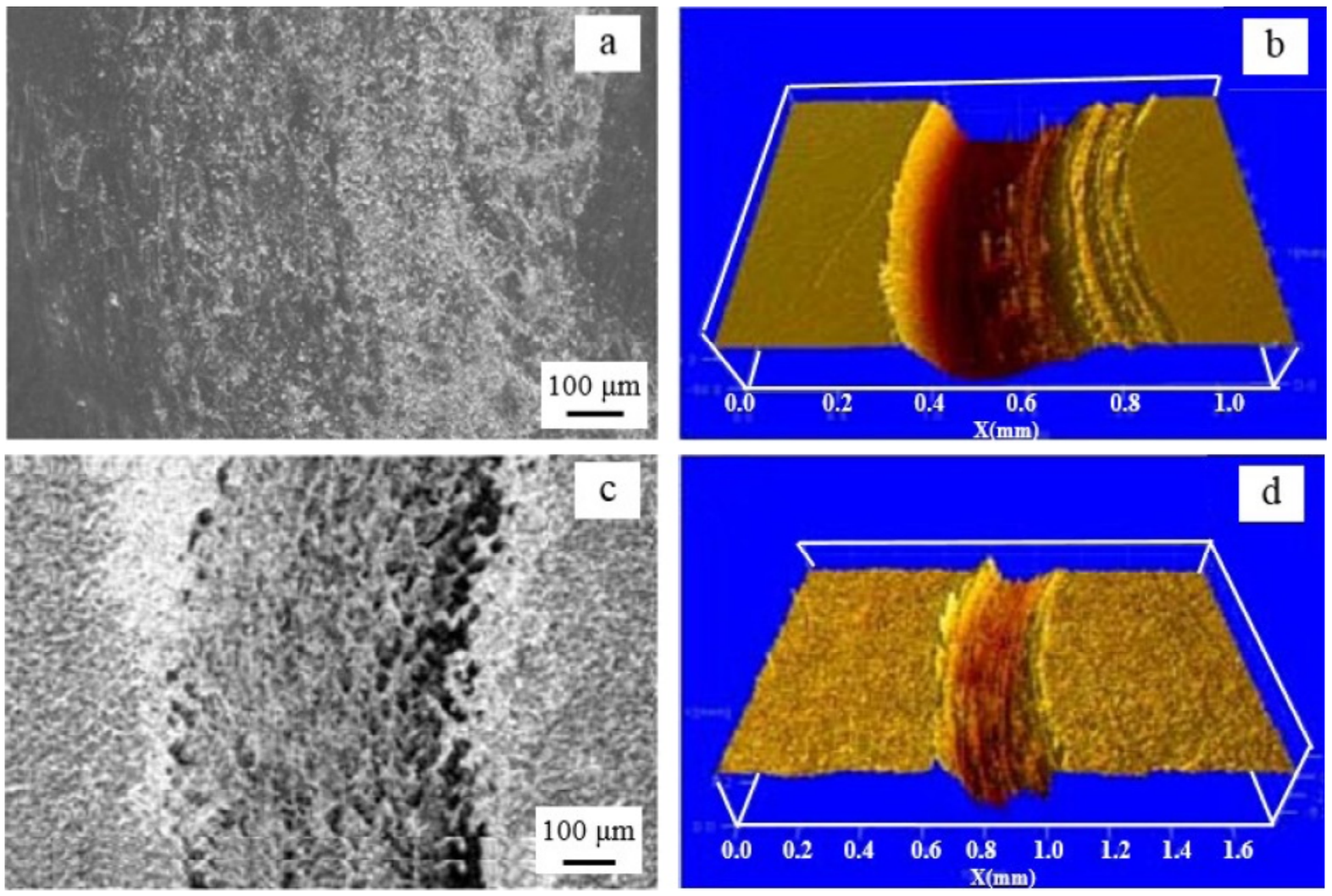

Fig. 33. SEM images and 3D surface profilometries of the wear traces at room temperature: (a), (b) TiAl; (c), (d) NiCr-O duplex layer.

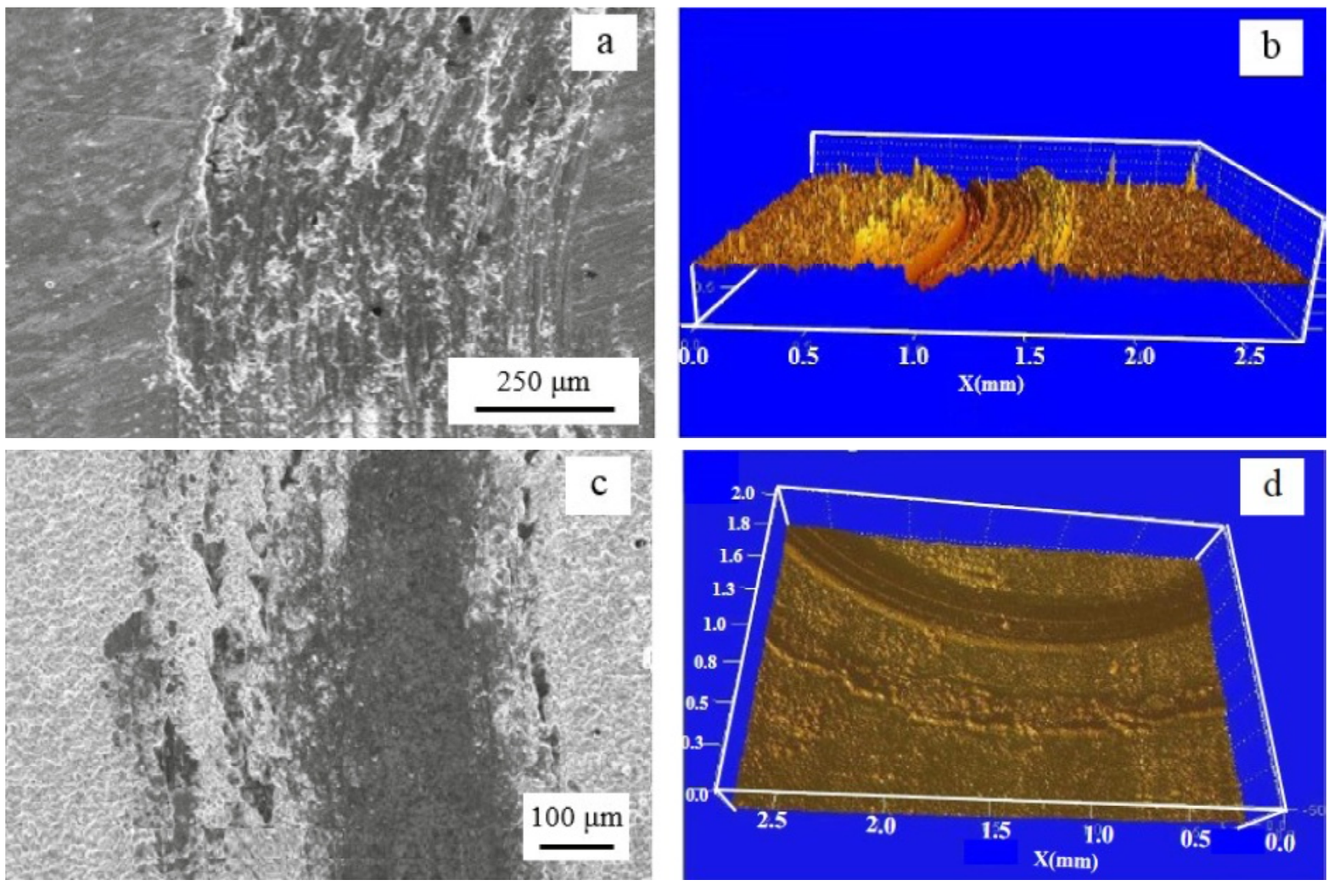

Fig. 34. SEM images and 3D surface profilometries of the wear traces at 773K: (a), (b) TiAl; (c), (d) NiCr-O duplex layer.

ing coating was beneficial to high-temperature oxidation resistance of the g-TiAl base alloy. Meanwhile NiCr-O composite alloying coating significantly improved the wear resistance of g-TiAl alloy at room temperature (Fig. 33) and 773K (Fig. 34) indicating by narrow and shallow wear traces.

Qiu et al. [111] fabricated a dense CrCoNiAlTiY coating on γ-TiAl alloy by DGPSA to improve its wear resistance. It was found that the obtained coating was continuous and compact with well diffusion bonded to the substrate (Figs. 35 and 36). Fig. 37 indicated that the CrCoNiAlTiY coating was composed of $AlCr_2$, σ-NiCoCr, γ-TiAl and γ'-Ni_3Al phases. In respect of the H/E and H^3/E^2 ratios, the CrCoNiAlTiY coating was almost 3.5 times better than those of the γ-TiAl substrate (Fig. 38). Dry wear test results showed that the specific wear rate of γ-TiAl substrate was 3.8×10^{-4} mm3 N^{-1} m^{-1}, which was about 4 times greater than that of the CrCoNiAlTiY coating (Fig. 39). The enhancement in

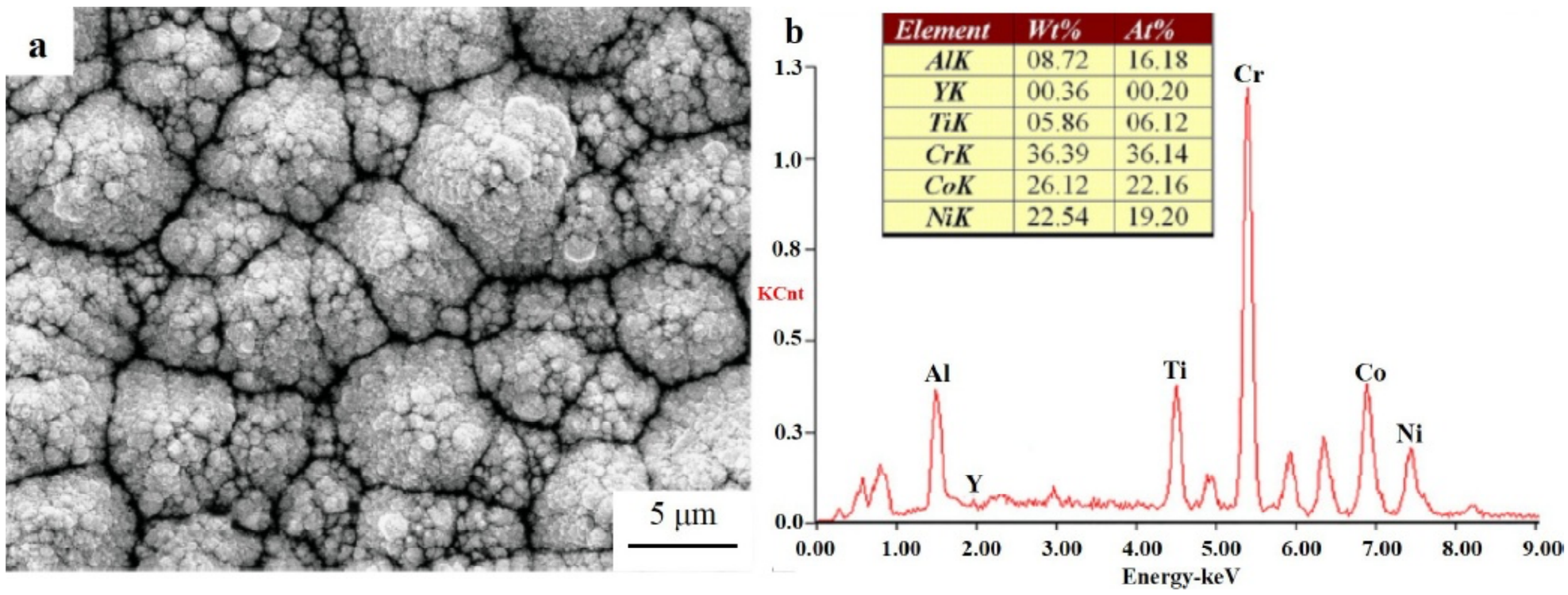

Fig. 35. SEM micrograph and the EDS analysis of the CrCoNiAlTiY coating: (a) surface morphology and (b) chemical composition.

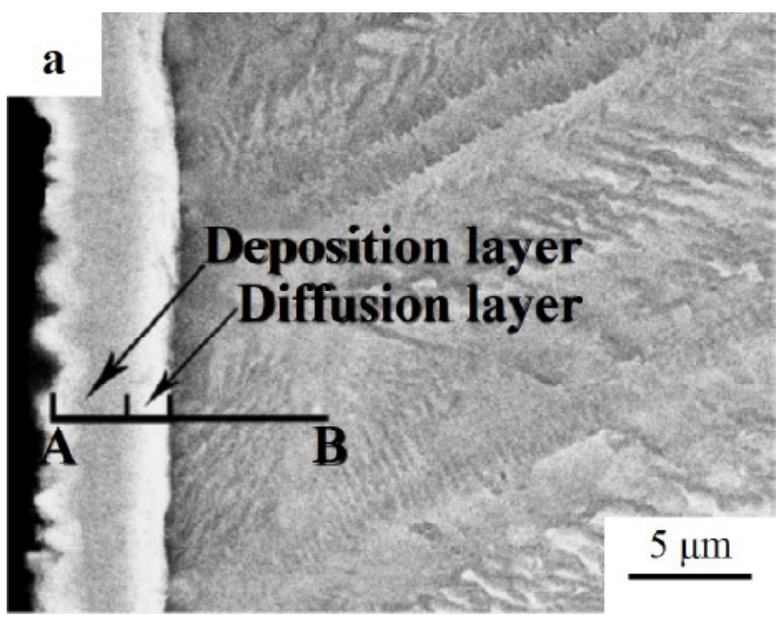

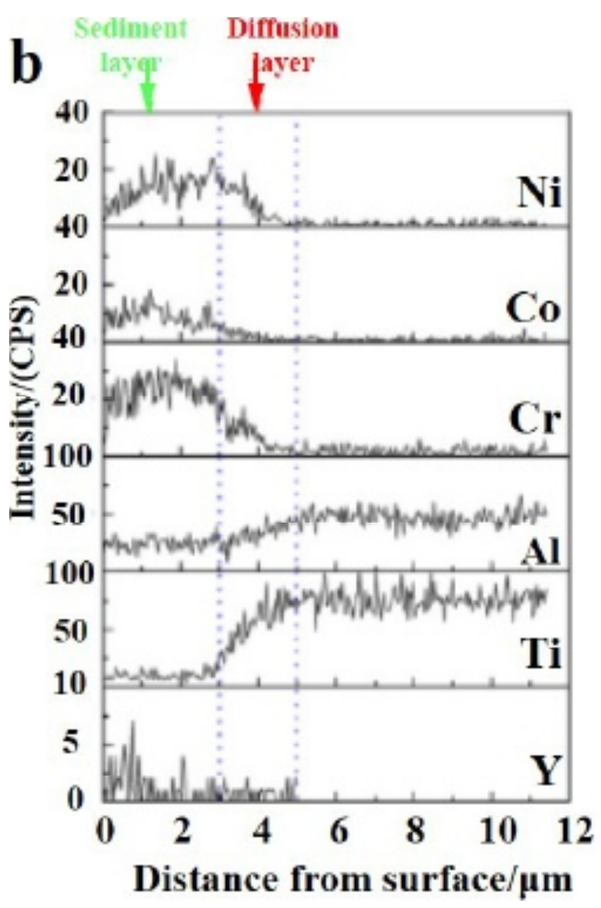

Fig. 36. SEM micrograph and the EDS analysis of the CrCoNiAlTiY coating: (a) cross-sectional microstructure, and (b) cross-sectional composition distribution.

wear resistance of the CrCoNiAlTiY coating might be attributed to the increased H/E and H^3/E^2 ratios and to the promising bonding strength between the CrCoNiAlTiY coating and the γ-TiAl substrate.

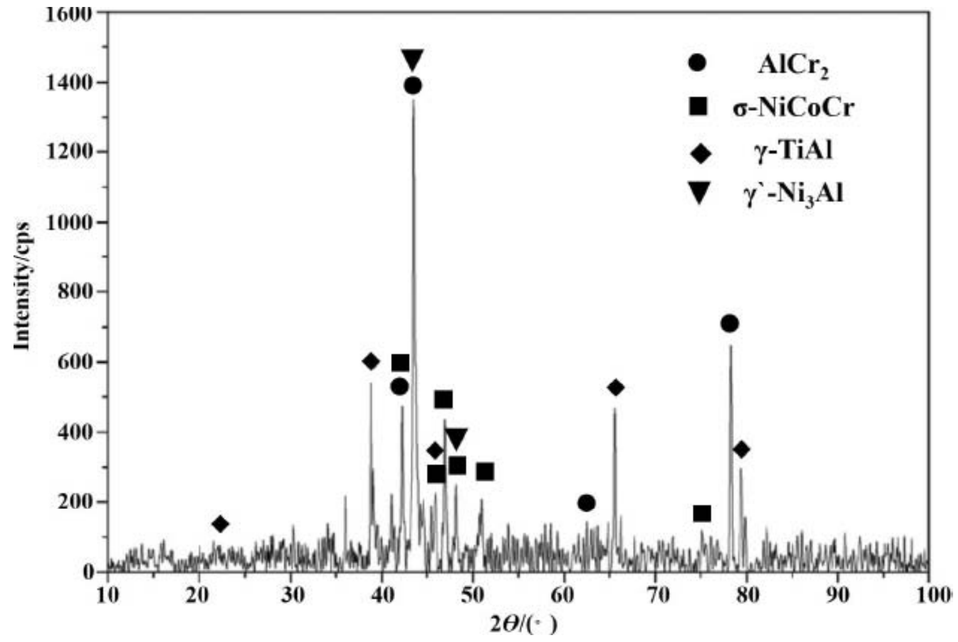

Fig. 37. XRD pattern of the CrCoNiAlTiY coating with identified phases.

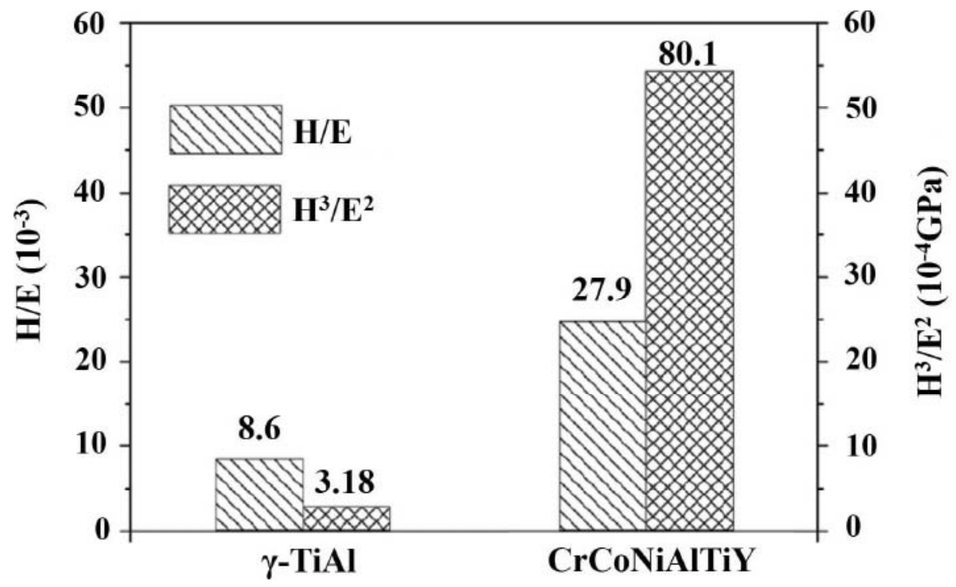

Fig. 38. H^3/E^2 and H/E ratios calculated form hardness and elastic modulus values for different samples.

4. SUMMARY

TiAl alloys are considered as a very important candidate material for advanced applications in aerospace, automotive, and related industries. Evidence from the literature showed that the nature/composition and hardness value of material surface play an important role in its corrosion and wear resistance. According to the literature, the improved tribologi-

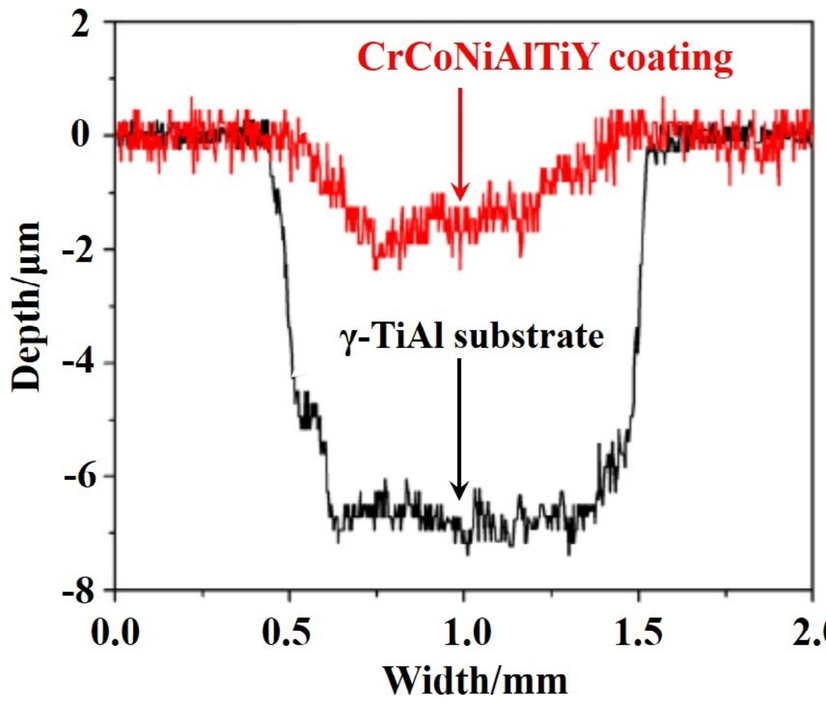

Fig. 39. The surface profilometry of wear scars of CrCoNiAlTiY coating and γ-TiAl substrate.

cal performance of TiAl alloys that achieved by DGPSA is due to the change in surface hardness and surface composition. Meanwhile, obtaining a strong metallurgical bond between the coating and the substrate benefits the surface performance. The positive roles in wear and corrosion behaviors of the selected alloying elements in alloyed layers lie in the following aspects: firstly formation of hard phases in the coating or in the near surface of TiAl alloys, receive a hard surface by obtaining intermetallic compounds, solid solution or dispersion strengthening on the near-surface of TiAl alloys; secondly the obtained alloyed surfaces can play a barrier or reduce oxygen diffusion effects and form a protective dense oxide scale with high bond strength with the substrate. In the long run, with the developments in design/processing and broadening practical applications of TiAl alloys, DGPSA will make a substantial contribution to refine or strengthen the surface performance and realize a favorable compromise between the cost and the performance of engineering components.

ACKNOWLEDGEMENT

This work was supported by the National Natural Science Foundation of China (No. 51474154 and No. 51501125), the China Postdoctoral Science Foundation (No.2012M520604 and No.2016M591415), the Natural Science Foundation for Young Scientists of Shanxi Province (No.2013021013-2 and No.2014011015-7), the Youth Foundation of Taiyuan University of Technology (No.2012L050, No.2013T011), and the Qualified Personnel Foundation of Taiyuan University of Technology (QPFT) (No. tyut-rc201157a). The authors would like to acknowledge valuable suggestions from Prof. Xiaoping Liu and Prof. Zhiyong He.

REFERENCES

[1] C. Liao, Y. He, J. Yang, B. Nan and X. Liu *// Mater. Sci. Eng. B* **178** (2013) 449.
[2] J. Lapin and T Pelachová // *Kovove Mater*. **42** (2004) 143.
[3] J. Lapin // *Kovove* Mater. **43** (2005) 81.
[4] I. Agote, J. Coleto, M. Gutiérrez, A. Sargsyan, M. García de Cortazar, M.A. Lagos, V.L. Kvanin, N.T. Balikhina, S.G. Vadchenko, I.P. Borovinskaya, A.E. Sytschev, L Pambaguian // *Kovove Mater.* **46** (2008) 87.
[5] Z Mirski and M. Rózańaski // *Arch. Civ. Mech. Eng.* **13** (2013) 415.
[6] M. Charpentier, D. Daloz and A. Hazotte // *Kovove Mater*. **50** (2012) 301.
[7] T. Kruml and K. Obrtlík // *Int. J. Fatigue* **65** (2014) 28.
[8] J. Lapin, A. Klimová and Z. Gabalcová // *Kovove Mater*. **51** (2013) 147.
[9] H. Clemens and S. Mayer // *Adv. Eng. Mater.* **15** (2013) 191.
[10] H. Clemens and H. Kestler // *Adv. Eng. Mater*. **2** (2000) 551.
[11] N.M. Lin, H.Y. Zhang, J.J. Zou and B. Tang // *Rev. Adv. Mater. Sci*. **38** (2014) 61.
[12] P.H. Mayrhofer, C. Mitterer. L. Hultman and H. Clemens // *Prog. Mater. Sci.* **51** (2006) 1032.
[13] Y.J. Jing, X.Y. Wang and J. Zhang // *Chin. J. Rare Met.* **33** (2009) 750.
[14] Y. Lu, J.B. Zhao and H.C. Qiao // *Chin. J. Lasers* **41** (2014) 1003013-1.
[15] H.C. Qiao, Y.X. Zhao, J.B. Zhao and Y. Lu // *Opt. Precis. Eng*. **22** (2014) 1766.
[16] M.Y. Zhang, K. Li, W. Zhang and T.H. Yao // *Mater. Sci. Eng. Powder Metall.* **18 (**2013) 552.
[17] C.G. Zhou, H.B. Xu, S.K. Gong, Y. Ying and Y.K. Kyoo // *Surf. Coat Technol.* **132** (2000) 117.
[18] X.L. Sun, P.D. Han, H.F. Li and Y.P. Liu // *Trans. Mater. Heat Treat*. **32** (2011) 127.
[19] G.J. Hwan, J.J. Dong and Y.K. Kyoo // *Surf. Coat Technol*. **154** (2002) 75.
[20] W. Liang, X.X. Ma, X.G. Zhao, J. Zhang and D.X. Zou // *Acta Metall. Sinica* **16** (2003) 466.
[21] R.R. Ahmad, P. Pejman, D. Naser and M.H. Seyed Mohammad // *Appl. Surf. Sci.* **276** (2013) 112.
[22] Z.D. Xiang, S. Rose and P.K. Datta // *Surf. Coat Technol*. **161** (2002) 286.
[23] H.P. Xiong, X.H. Li, W. Mao, J.P. Li, W.L. Ma and Y.Y. Cheng // *Acta Metall. Sinica* **39** (2003) 66.

[24] Y. Jiang, Y.H. He, Y.W. Tang, Z. Li and B.Y. Huang // *Chin. J. Mater. Res.* **19** (2005) 139.
[25] B. Zhao, J.S. Wu, J. Sun and F. Wang // *Acta Metall. Sinica* **37** (2001) 837.
[26] X.Q. Wu, F.Q. Xie, Z.C. Hu and L. Wang // *Trans. Nonferrous Met. Soc. China* **20** (2010) 1032.
[27] J.M. Hao, W.Q. Jie, H. Chenand and Y.D. Ye // *Rare Met. Mater. Eng*. **34** (2005) 1455.
[28] X.J. Li, X.L. Wu, W.B. Xue, G.A. Cheng, R.T. Zheng and Y.J. Cheng // *Surf. Coat Technol.* **201** (2007) 5556.
[29] H.P. Xiong, W. Mao, W.L. Ma, Y.Y. Cheng, J.P. Li and X.H. Li // *Acta Metall. Sinica* **39** (2003) 744.
[30] X.J. Li, G.A. Cheng, W.B. Xue, R.T. Zheng, H. Tian and Y.J. Cheng // *Mater. Sci. Eng. Powder Metall*. **14** (2009) 115.
[31] J.K. Lee, H.N. Lee, H.K. Lee, M.H. Oh and D.M. Wee // *Surf. Coat. Technol.* **155** (2002) 59.
[32] J.P. Kim, H.G. Jung and K.Y. Kim // *Surf. Coat. Technol*. **112** (1999) 91.
[33] S.K. Gong, H.B. Xu, Q.H. Yu and C.G. Zhou // *Surf. Coat. Technol.* **130** (2000) 128.
[34] H.Q. Li, Q.M. Wang, J. Gong and C. Sun // *Appl. Surf. Sci*. **257** (2011) 4105.
[35] S Narksitipan., T. Thongtem and S. Thongtem // *Appl. Surf. Sci*. **254** (2008) 7759.
[36] M. Miyake, S. Tajikara and T. Hirato // *Surf. Coat. Technol.* **205** (2011) 5141.
[37] U. Mikito, S. Daigo, K. Shoichi and O. Toshiaki // *Surf. Coat. Technol.* **176** (2004) 202.
[38] J. Gao, Y. He and W. Gao // *Surf. Coat. Technol.* **205** (2011) 4453.
[39] X.X. Ma, Y.D. He and D. R. Wang // *Appl. Surf. Sci.* **257** (2011) 10273.
[40] T. Sasaki, T. Yagi, T. Watanabe and A. Yanagisawa // *Surf. Coat. Technol*. **205** (2011) 3900.
[41] W.B. Li, S.L. Zhu, M.H. Chen, C. Wang and F.H. Wang // *Appl. Surf. Sci.* **292** (2014) 583.
[42] J.K. Lee, H.N. Lee, H.K. Lee, M.H. Oh and D.M. Wee // *Surf. Coat. Technol*. **182** (2004) 363.
[43] X.J. Zhang, C.X. Gao, L. Wang, Q. Li, S.J. Wang and Y. Zhang // *Rare Met. Mater. Eng.* **39** (2010) 367.
[44] X. Tian, Q. Jia, Y.Y. Cui and R. Yang // *The Chin. J. Nonferrous Met.* **20** (2010) S264.
[45] B.Y. Ren, X.J. Zhang, N.X. Feng and F. Gao // *The Chin. J. Nonferrous Met*. **19** (2009) 1488.
[46] Z.W. Li, W. Gao, M. Yoshihara and Y.D. He // *Mater. Sci. Eng*. **A347** (2003) 243.
[47] Z.W. Li, W. Gao and Y.D. He // *Scr. Mater*. **45** (2001) 1099.
[48] Y. Chen, H.M. Wang // *Appl. Surf. Sci*. **220** (2003) 186.
[49] X.B. Liu, S.H. Shi, J. Guo, G.Y. Fu and M.D. Wang // *Appl. Surf. Sci.* **255** (2009) 5662.
[50] X.B. Liu and H.M. Wang // *Appl. Surf. Sci*. **252** (2006) 5735.
[51] U. Hornauer, E. Richter, W. Matz, H. Reuther, A. Mücklich, E. Wieser, W. Möller, G. Schumacher and M. Schütze // *Surf. Coat. Technol*. **128-129** (2000) 418.
[52] U. Hornauer, E. Richter, E. Wieser, W. Möller, A. Donchev and M. Schütze // *Surf. Coat. Technol.* **174-175** (2003) 1182.
[53] Y.C. Zhu, X.Y. Li, K. Fujita, N. Iwamoto, Y. Matsunaga, K. Nakagawa and S. Taniguchi // *Surf. Coat. Technol*. **158-159** (2002) 503.
[54] J. Xia, C.X. Li, H. Dong and T. Bell // *Surf. Coat. Technol*. **200** (2006) 4755.
[55] B. Chatdanai and T. Somchai // *Appl. Surf. Sci.* **256** (2009) 484.
[56] N. Suparut, T. Titipun, M. Michael and T. Somchai // *Appl. Surf. Sci*. **252** (2006) 8510.
[57] Y.C. Chen and J. C. Feng // *Rare Met. Mater. Eng.* **34** (2005) 1969.
[58] Y.C. Chen and J. C. Feng // *The Chin. J. Nonferrous Met.* **14** (2004) 1839.
[59] H.Z. Li, Z. Li, M. Zeng, Y. Liu, W. Zhang and L.G. Han // *J. Cent. South Univer.* **42** (2011) 629.
[60] M. Fröhlich, R. Braun and C. Leyens // *Surf. Coat. Technol.* **201** (2006) 3911.
[61] W.W. Chen and Y.D. He // *Trans. Mater. Heat Treat.* **32** (2011) 138.
[62] D.S. Wang, Z.J. Tian, Z.Y. Chen, L.D. Shen, Z.D. Liu and Y.H. Huang // *J. Mater. Eng.* **22** (2009) 72.
[63] X.J. Li, G.A. Cheng, W.B. Xue, R.T. Zheng, X.L. Wu and Y.J. Cheng // T*rans. Mater. Heat Treat.* **27** (2009) 95.
[64] M. Aliofkhazraei, A. Sabour Rouhaghdam and H. Hassannejad // *Rare Met.* **28** (2009) 454.
[65] J. Xu, X.S. Xie and Z. Xu // *J. Mater. Sci. Technol*. **19** (2003) 404.
[66] Z. Xu, L. Qin, , B. Tang and Z.Y. He // *Acta Metall. Sinica* **15** (2002) 172.

[67] Z. Xu, X. Liu, P. Zhang, Y. Zhang, G. Zhang and Z. He // *Surf. Coat. Technol*. **201** (2007) 4822.
[68] S.J. Ma, P.Z. Zhang, Q. Miao and Z. Xu // *Heat Treat. Met*. **22** (2007) 26.
[69] C.Y. Yuan, W.P. Liang, Q. Miao, Z.J. Yao, P.Z. Zhang and Y.D. Jiang // *Rare Met. Cement. Carbide* **38** (2010) 28.
[70] J.J. Yang, Q. Miao, W.P. Liang, L. Li, B.L. Ren and D.Y. Zhu // *Heat Treat. Met.* **38** (2013) 110.
[71] C.L. Zheng, X.S. Xie, J.X. Dong, Z. Xu and Z.Y. He // *Aerosp. Mater. Technol*. **23** (2002) 51.
[72] X.F. Wang, Y. Fan, Z.X. Wang and Z.Y. He // *Phys. Test. Chem. Anal. Part A Phys. Test.* **44** (2008) 57.
[73] S.J. Ma, P.Z. Zhang, H.Y. Wu and Z. Xu // *Heat Treat. Met*. **33** (2008) 67.
[74] Z.Y. He, Z.X. Wang, X.P. Liu and P.D. Han // *Vacuum* **89** (2013) 280.
[75] Z.Y. He, Z.X. Wang, F. Zhang, Z.Y. Wang and X. P. Liu // *Surf. Coat. Technol*. **228** (2013) S287.
[76] W.P. Liang, Z. Xu, Q. Miao, X.P. Liu and Z.Y. He // *Tribology* **27** (2007) 121.
[77] H.Y. Wu, P.Z. Zhang, L. Wang, H.F. Zhao and Z. Xu // *Appl. Surf. Sci.* **256** (2009) 1333.
[78] H.Y. Wu, P.Z. Zhang, S.J. Ma and Z. Xu // *Lubr. Eng.* **32** (2007) 68.
[79] H.Y. Wu, P.Z. Zhang, J.L. Li, S.J. Ma and Z. Xu // *The Chin. J. Nonferrous Met.* **17** (2007) 1656.
[80] H.Y. Wu, P.Z. Zhang, J.L. Li, G. Hussain and Z. Xu // *Tribol. Lett.* **30** (2008) 61.
[81] H.Y. Wu, P.Z. Zhang and Z. Xu // *J. Wuhan Univer. Technol.-Mater. Sci. Ed.* **24** (2009) 106.
[82] W.P. Liang, Z. Xu, Q. Miao, X.P. Liu and Z.Y. He // *Chin. J. Aeronaut.* **19** (2006) 255.
[83] W.P. Liang, Z. Xu, Q. Miao, X.P. Liu and Z.Y. He // *Rare Met. Mater. Eng.* **35** (2006) 1826.
[84] X.P. Liu, Z. Xu, W. Xu, W.P. Liang, C.L. Guo and W.H. Tian // *Trans. Nonferrous Met. Soc. China* **15** (2005) 420.
[85] W. Xu, X.P. Liu and Z. Xu // *Hot Working Technol.* **37** (2008) 109.
[86] W. Xu and X.P. Liu // *Total Corros. Control* **24** (2010) 23.
[87] C.L. Guo, H.F. Ben, X.P. Liu and P.Z. Zhang // *Hot Working Technol.* **36** (2007) 57.
[88] C.L. Zheng, F.Z. Cui, Z. Xu, X.S. Xie and Z.Y. He // *Surf. Coat. Technol*. **174-175** (2003) 1014.
[89] D.D. Chen, W.H. Tian, J. Wang and X.P. Liu // *J. Univer. Sci. Technol. Beijing* **15** (2008) 590.
[90] X.P. Liu, P.L. Ge, K. You, Z.X. Wang and Z.Y. He // *Rare Met. Mater. Eng*. **40** (2011) 1891.
[91] H.Y. Wu, Y. Li, X. Tang, G. Hussain, H.F. Zhao and Q.F. Li // *Appl. Surf. Sci.* **324** (2015) 160.
[92] H.Y. Wu and P.Z. Zhang // *Rare Met. Mater. Eng.* **36** (2007) 846.
[93] Y.F. Li, P. Z. Zhang and H. Xu // *Rare Met. Cement. Carbide* **40** (2012) 36.
[94] Y.F. Li, P. Z. Zhang and H. Xu // *J. Aeronaut. Mater.* **31** (2011) 43.
[95] Y.F. Li, P. Z. Zhang, K. Lin and J.W. Yu // *Mater. Rev.* **25** (2011) 90.
[96] Y.F. Li, P. Z. Zhang, C. Li and J.W. Yu // *Rare Met. Cement. Carbide* **39** (2011) 38.
[97] H.F. Ben, C.L. Guo and X.P. Liu // *New Technol. New Process* **27** (2007) 79.
[98] F. Xing, *M.A. thesis* (Taiyuan University of Technology, Taiyuan, 2012).
[99] X.P. Liu, W.H. Tian, W. Xu, W.P. Liang and Z. Xu // *Surf. Coat. Technol.* **201** (2007) 5278.
[100] C.L. Guo, X.P. Liu, H. F. Ben and Z.Y. He // *Surf. Coat. Technol*. **202** (2008) 1797.
[101] B.Y. Wang, J. Zhang and X. M. Yuan // *Surf. Technol*. **40** (2011) 45.
[102] B.Y. Wang, J. Zhang and X. M. Yuan // *J. Luoyang Inst. Sci. Technol.* **22** (2012) 10.
[103] H.Y. Wu, P.Z. Zhang, W. Chen, L. Wang, H.F. Zhao and Z. Xu // *Trans. Nonferrous Met. Soc. China* **19** (2009) 1121.
[104] D.D. Zheng, *Master Thesis* (Nanjing University of Aeronautics and Astronautics, Nanjing, 2010).
[105] X.F. Wei, P.Z. Zhang, D.B. Wei, X.H. Chen, Q. Wang and R.N. Wang // *Acta Metall. Sinica* **49** (2013) 1406.
[106] X.F. Wei, P.Z. Zhang, D.B. Wei, L.L. Shan, P. Zhou and Y. Zhang // *Mater. Mech. Eng.* **33** (2014) 12.
[107] Y. Fan, *Master Thesis* (Taiyuan University of Technology, Taiyuan, 2008).
[108] Y. Huang, P.Z. Zhang, D.B. Wei and J. Huang // *Heat Treat. Met*. **37** (2012) 58.
[109] H.Y. Wu, P.Z. Zhang, H.F. Zhao, L. Wang and A.G. Xie // *Appl. Surf. Sci*. **257** (2011) 1835.
[110] Y. Huang, Master Thesis (Nanjing University of Aeronautics and Astronautics, Nanjing, 2012).
[111] Z.K. Qiu, P.Z. Zhang, D.B. Wei, B.Z. Duan and P. Zhou // *Tribol. Inter.* **92** (2015) 512–518.